UNIVERSITY OF CALIFORNIA SAN DIEGO

TRIM1, Rab32 and Rab38 are novel regulators of LRRK2 localization and kinase activity

A Thesis submitted in partial satisfaction of the requirements
for the degree Master of Science

in

Biology

by

Jacob Porath

Committee in charge:

Professor Annie Hiniker, Chair
Professor James Kadonaga, Co-Chair
Professor Stacey Glasgow

2023

The Thesis of Jacob Porath is approved, and it is acceptable
in quality and form for publication on microfilm and electronically.

University of California San Diego
2023

TABLE OF CONTENTS

LIST OF FIGURES

ACKNOWLEDGEMENTS

Firstly, I must thank my PI Dr. Annie Hiniker for opening the door to biology research for me and for her constant guidance over my nearly 4 years at the Hiniker Lab. I am also very grateful to Alexandra Unapanta for her extensive support of both my writing and my research. I must also thank Farbod Shavarebi who served as my mentor in my early research at the Hiniker Lab and who continues to provide guidance to me now. Finally, I would like to thank the remaining members of the Hiniker Lab for a number of experimental insights that made this project possible.

ABSTRACT OF THE THESIS

TRIM1, Rab32 and Rab38 are novel regulators of LRRK2 localization and kinase activity

by

Jacob Porath

Master of Science in Biology

University of California San Diego, 2023

Professor Annie Hiniker, Chair
Professor James Kadonaga, Co-Chair

Parkinson's Disease (PD) is the second most common neurodegenerative disorder, currently affecting over 7 million individuals worldwide. Clinically, PD results in progressive cell death of dopaminergic neurons in the basal ganglia and substantia nigra, but what drives this cell death is still unclear. Point mutations to the Leucine-Rich Repeat Kinase 2 (LRRK2) gene are the most common cause of inherited PD and importantly, LRRK2-PD phenocopies sporadic PD. Thus, better understanding the roles of the LRRK2 protein could provide insights into the driving forces behind PD pathogenesis and progression.

LRRK2 has several protein interaction domains and has been shown to be regulated by a number of interactors, yet adequate characterization of the LRRK2 protein interactome is still

lacking. Chapter 1 will provide a comprehensive background on LRRK2 biology detailing its structure, function and interactions to inform topics explored in subsequent chapters. Chapter 2 identifies the E3 ubiquitin ligase TRIM1 as a novel regulator of LRRK2 microtubule localization and LRRK2 degradation by the proteasome. Chapter 3 comprises the first report of endogenous regulation of LRRK2 by a Rab protein. Endogenous Rab38 regulates LRRK2 subcellular localization in B16-F10 mouse melanocytes. Finally, Chapter 4 explores the effects of chloroquine and IFN-γ treatment on LRRK2 localization and activity in macrophages. This chapter reveals a novel interaction between LRRK2 and Rab32 in RAW 264.7 macrophages under IFN-γ treatment. These results highlight the need for further research into LRRK2 protein interactors which could regulate LRRK2 activity through a number of mechanisms in a cell-type specific manner.

Chapter 1: Review of LRRK2 biology

Mutations to the Leucine-Rich Repeat Kinase 2 (LRRK2) gene are the most common mutations among patients with familial Parkinson's Disease (PD). PD results in cell death of dopaminergic neurons in the basal ganglia and substantia nigra, but what drives this cell death is still unclear. This causes PD patients to suffer from tremors, rigidity and slowness of movement among other motor and nonmotor symptoms. The age of onset is around 60 years on average and symptoms typically manifest after the loss of 50-80% of dopaminergic neurons, making it difficult to diagnose before the disease has progressed quite substantially (1). The other central physiological manifestation of PD is the formation of Lewy Bodies (LB) which are intracellular aggregates of alpha-synuclein (αSyn), ubiquitin and other proteins (2). Interestingly, certain LRRK2 mutants such as G2019S exhibit typical Lewy pathology, whereas others such as I2020T right next to it very rarely display Lewy pathology (3). LBs accumulate in dopaminergic neurons of the substantia nigra in PD patients and mutations to αSyn have been shown to cause aggregation, making αSyn a strong target for possible PD therapeutics (4, 5). Currently, PD therapeutics are largely limited to the treatment of symptoms rather than the disease itself, and treatments for nonmotor symptoms are also lacking (6, 7). Beyond research into therapeutics, work is being done to identify biomarkers of PD which can be used to identify the disease early and thus open the door for neuroprotective treatment to prevent disease progression (6).

PD is the second most common neurodegenerative disorder currently affecting over 7 million people worldwide with age clearly being the greatest risk factor (8, 9). Familial PD accounts for just 5-10% of total cases and there are six genes which have been definitively linked to PD: LRRK2 and SNCA (αSyn) linked to autosomal-dominant PD and Parkin, PINK1, DJ-1 and ATP13A2 linked to autosomal-recessive PD (10). There are around 50 known mutations to

the LRRK2 gene, of which a handful are known to be pathogenic (10). These pathogenic LRRK2 mutations are responsible for up to 5% of familial PD cases and 1-2% of sporadic PD cases, but these numbers can reach as high as 40% of cases in certain populations (11, 12). Although LRRK2-related PD cases make up a small proportion of the total, LRRK2 PD symptoms closely resemble sporadic PD symptoms. Therefore, understanding the mechanism behind LRRK2 driven PD could provide valuable insights into PD development and progression more broadly.

The role of the LRRK2 protein appears to be widespread with high expression in immune, lung, kidney and intestine cells (13). Somewhat surprisingly, LRRK2s expression in the brain is quite low with the highest levels in the putamen, which is a target of the substantia nigra, and just detectable levels are found in the substantia nigra itself (14). In the immune system LRRK2 exhibits high expression in neutrophils, monocytes and macrophages, contributing to cytokine release, autophagy and phagocytosis (15). LRRK2 plays an important role in the endolysosomal system where it is recruited to lysosomes upon overload stress (16). Further, LRRK2-PD mutants result in lysosomal enlargement and a reduction in degradative function (17). LRRK2 also contributes to intracellular transport along microtubules through phosphorylation of its substrates in the membrane-trafficking Rab protein family (18). As a result of LRRK2's widespread functions, mutations in LRRK2 are implicated as risk alleles in a number of diseases beyond PD including Crohn's, leprosy and tuberculosis (19, 20, 21).

LRRK2 is a relatively large protein (288 kDa, 2527 amino acids), containing multiple protein interaction and catalytic domains. The protein interaction domains are situated on the amino-terminal half of the protein, being the Armadillo, Ankyrin and Leucine-Rich Repeat domains. The catalytic domains on the carboxy-terminal half are the Ras-of-Complex (RoC), C-Terminal of Roc (COR) and the Kinase domain. Finally, there is a WD40 protein interaction

domain on the far carboxy-terminal end (18). Structurally, this catalytic half of the protein folds over onto itself in a rough J-shape situating the Roc and COR regions next to the Kinase domain. This allows for interaction between the kinase domain and GTPase domain, facilitating LRRK2 binding to GTP which is essential for LRRK2 kinase activity (22). Additionally, this crosstalk between domains can also occur via dimerization through COR/COR or WD40/WD40 interactions (18).

LRRK2 pathogenic mutants are primarily those which result in increased kinase activity. The most common pathogenic LRRK2 mutation is the G2019S mutation in LRRK2's catalytic domain, which is especially prevalent in certain communities such as Ashkenazi Jews or North African Berbers, where it makes up 30-41% of cases (12). Another notable mutation which occurs in the catalytic domain is the I2020T mutation, which is especially prevalent in the Japanese population and was actually the first LRRK2 mutant definitively linked to PD (23, 24). Unsurprisingly, I2020T increases LRRK2 kinase activity through a similar mechanism to G2019S. These catalytic domain mutants work through disruption of an important hydrogen bond at Tyr2018 of the protein's DYG motif, which is thought to stabilize LRRK2 in a less active open conformation (25). This releases the metaphorical brake on LRRK2 activity, inhibiting its dynamic kinase switch mechanism (25). The G2019S mutation has been shown to increase kinase activity by 2-3 times through this mechanism (26).

Another important subset of LRRK2 PD mutants resides in the Roc and COR domains. LRRK2 mutations such as R1441G/C/H, Y1699C and N1437H result in PD pathogenesis by promoting LRRK2/GTP binding and by suppression of GTPase activity. Interestingly, R1441G is an especially common mutation among PD patients in the Basque region of Spain, appearing in 16%-22% of familial cases and 4% of sporadic cases (27, 28). The importance of this domain to

LRRK2-PD is underscored by the high number of relevant mutations here compared to just 2 in the catalytic domain (29). Further, the penetrance of these mutations is quite high with the R1441 mutants having over 90% penetrance past the age of 75, compared to just 25-40% with G2019S for example (30, 31). These ROC-COR pathogenic mutants have been shown to increase LRRK2 kinase activity by roughly 3-4 times (32).

There are a number of factors which alter LRRK2's kinase activity, with one of the most important being its localization. LRRK2 is found in numerous locations within the cell depending on context such as the cytoplasm, membrane surfaces and microtubules. The majority of LRRK2 is found in the cytoplasm where it binds to 14-3-3 protein, dependent on the phosphorylation of LRRK2 residues S910 and S935 (33, 34). The pathogenic LRRK2 mutants R1441G/C, Y1699C and I2020T have reduced S910 and S935 phosphorylation, resulting in limited 14-3-3 binding (35). 14-3-3 seems to maintain diffuse LRRK2 localization throughout the cytoplasm whereas mutants with reduced 14-3-3 binding accumulate into large cytoplasmic aggregates or localize to the microtubules (34, 35).

Previous research shows that roughly 10-25% of LRRK2 is present at the membrane and membrane-bound LRRK2 typically exists in its dimer form which is far more active (33, 36). In fact, membrane-bound LRRK2 is ~3 times as active as cytosolic LRRK2 likely due to dimerization and enhanced GTP binding (36). LRRK2 associates with a number of membrane-bound organelles such as the trans-golgi network and membrane-bound vesicles, where it can phosphorylate a subset of Rab GTPases--proteins which have understudied relationships with LRRK2 and may be important interactors affecting LRRK2 function (26).

LRRK2 can also directly associate with microtubules in an oligomeric right-handed helix structure, but it must be in a closed (active) conformation to bind (18). It is a direct attachment

relying on the C-terminal half to form microtubule-associated filaments. LRRK2's association with microtubules may have ties to PD progression because 4 of the 5 major pathogenic mutants have increased microtubule association (18). The neuronal cytoskeleton seems to be a critical area for studying neurodegeneration because many proteins implicated in neurodegeneration, such as LRRK2, αSyn and parkin can either bind tubulin or affect microtubule stability (36). One instance of LRRK2 pathology affecting the microtubules is reduced neurite outgrowth in response to pathogenic LRRK2 mutation, indicating a LRRK2 induced defect in cytoskeletal structure (36). Interestingly, research that I have contributed to shows that the TRIM1 protein can recruit LRRK2 to the microtubules and even rescue the neurite outgrowth defect, making it a critical regulator of LRRK2 function (37). This will be discussed in more detail in Chapter 2.

Because enhanced LRRK2 kinase activity is so strongly associated with PD pathogenesis, LRRK2 kinase inhibitors have been explored as a potential PD therapeutic. However due to LRRK2's broad range of functions, kinase inhibitors may negatively impact other areas where LRRK2 kinase activity is vital such as the lungs and kidneys (38). This lung and kidney phenotype is also observed in LRRK2-deficient mice, suggesting that this is simply an effect of LRRK2 inhibition rather than a side-effect of drug treatment (39). However, the lung and kidney effect generally appears mild and reversible (40). Pairing this finding with research showing that humans with genetically reduced LRRK2 levels show no clear health defects suggests that partial LRRK2 inhibition could be a future therapy option (41).

Despite LRRK2's great importance to PD research, several aspects of its cellular mechanisms remain understudied. One such area of intrigue central to this project is LRRK2's interaction with its substrates. Although there is speculation about many possible substrates of LRRK2, a subset of Rab GTPases are the only validated physiological substrates of LRRK2 (26).

These Rab proteins are of great interest because previous research has shown that the Rab29 protein can recruit LRRK2 to the trans-golgi network where it increases LRRK2 kinase activity substantially and, as mentioned, increases in LRRK2 kinase activity are linked to PD pathogenesis (33). Building on this, the Rab32 and Rab38 proteins share a high degree of homology with Rab29 making them great candidates as possible regulators of LRRK2 kinase activity and thus, important proteins to LRRK2 and PD biology. Due to their homology, Rab29, Rab32 and Rab38 are considered a subfamily within the Rab superfamily with Rab32 sharing 56% identity with Rab29 and Rab38 sharing 52% identity with Rab29. Interestingly, Rab38-deficient mutant rats have increased surfactant buildup in the lungs, an area with high Rab38 and LRRK2 expression. This surfactant buildup also occurs with LRRK2 kinase inhibitor treatment, which suggests LRRK2's involvement in this pathway as well (38, 42). Therefore, there are likely novel Rab-LRRK2 interactions which could be valuable to the understanding and treatment of PD. The identification of novel Rab regulators of LRRK2 function is the subject of Chapter 3.

Mutations to the LRRK2 protein are responsible for a substantial number of both familial and idiopathic PD cases. Understanding the effects of LRRK2 dysfunction is critical to helping these LRRK2-PD patients and could give valuable insights into the pathologic mechanism behind PD as a whole. Therefore, research into understudied areas of LRRK2 biology such as its localization and substrate interactions is essential. Chapter 2 will explore LRRK2's relationship with the TRIM1 protein and its effect on LRRK2 localization and degradation. Chapter 3 will explore Rab38's regulation of LRRK2 subcellular localization. Finally, Chapter 4 will explore the effects of IFN-γ and chloroquine treatment on LRRK2 localization and activity, while revealing an interaction between LRRK2 and Rab32 in IFN-γ treated RAW 264.7 macrophages.

Figure 1.1: LRRK2 structure and domain organization. The domains are ARM (Armadillo), ANK (Ankyrin), LRR (Leucine-Rich Repeat), ROC (Ras-of-Complex), COR (C-terminal of Roc), Kinase and WD40. The most common pathogenic LRRK2-PD mutants are labeled above. The catalytic domains and protein interaction domains are also specified below. Adapted from Usmani et al., 2017.

Figure 1.1

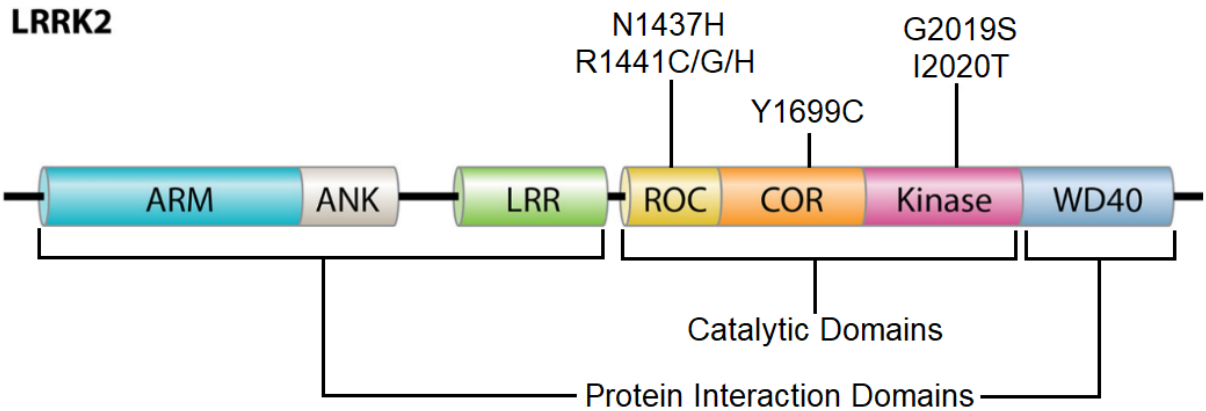
LRRK2
N1437H
R1441C/G/H
G2019S
I2020T
Y1699C
ARM
ANK
LRR
ROC
COR
Kinase
WD40
Catalytic Domains
Protein Interaction Domains

References

1. DeMaagd, G., & Philip, A. (2015). Parkinson's Disease and Its Management: Part 1: Disease Entity, Risk Factors, Pathophysiology, Clinical Presentation, and Diagnosis. *P & T : a peer-reviewed journal for formulary management*, *40*(8), 504–532.

2. Rocha Cabrero, F., & Morrison, E. H. (2022). Lewy Bodies. In *StatPearls*. StatPearls Publishing

3. Kalia, L. V., Lang, A. E., Hazrati, L.-N., Fujioka, S., Wszolek, Z. K., Dickson, D. W., Ross, O. A., Van Deerlin, V. M., Trojanowski, J. Q., Hurtig, H. I., Alcalay, R. N., Marder, K. S., Clark, L. N., Gaig, C., Tolosa, E., Ruiz-Martínez, J., Marti-Masso, J. F., Ferrer, I., López de Munain, A., Goldman, S. M., Schüle, B., Langston, J. W., Aasly, J. O., Giordana, M. T., Bonifati, V., Puschmann, A., Canesi, M., Pezzoli, G., Maues De Paula, A., Hasegawa, K., Duyckaerts, C., Brice, A., Stoessl, A. J., Marras, C. (2015). Clinical correlations with Lewy body pathology in LRRK2-related Parkinson disease. *JAMA Neurology*, *72*(1), 100. https://doi.org/10.1001/jamaneurol.2014.2704

4. Yasuda, T., & Mochizuki, H. (2010). The regulatory role of α-synuclein and parkin in neuronal cell apoptosis; possible implications for the pathogenesis of Parkinson's disease. *Apoptosis : an international journal on programmed cell death*, *15*(11), 1312–1321. https://doi.org/10.1007/s10495-010-0486-8

5. Rohn T. T. (2012). Targeting alpha-synuclein for the treatment of Parkinson's disease. *CNS & neurological disorders drug targets*, *11*(2), 174–179. https://doi.org/10.2174/187152712800269678

6. Smith, Y., Wichmann, T., Factor, S. A., & DeLong, M. R. (2011). Parkinson's disease therapeutics: New developments and challenges since the introduction of levodopa. *Neuropsychopharmacology*, *37*(1), 213–246. https://doi.org/10.1038/npp.2011.212

7. Cabreira, V., & Massano, J. (2019). Parkinson’s Disease: Clinical Review and Update. *Acta Médica Portuguesa*, *32*(10), 661–670. https://doi.org/10.20344/amp.11978

8. de Lau, L. M. L., & Breteler, M. M. B. (2006). Epidemiology of parkinson's disease. *The Lancet Neurology*, *5*(6), 525–535. https://doi.org/10.1016/s1474-4422(06)70471-9

9. Pringsheim, T., Jette, N., Frolkis, A., & Steeves, T. D. L. (2014). The prevalence of parkinson's disease: A systematic review and meta-analysis. *Movement Disorders*, *29*(13), 1583–1590. https://doi.org/10.1002/mds.25945

10. Klein, C., & Westenberger, A. (2012). Genetics of parkinson's disease. *Cold Spring Harbor Perspectives in Medicine*, *2*(1). https://doi.org/10.1101/cshperspect.a008888

11. Gilks, W. P., Abou-Sleiman, P. M., Gandhi, S., Jain, S., Singleton, A., Lees, A. J., Shaw, K., Bhatia, K. P., Bonifati, V., Quinn, N. P., Lynch, J., Healy, D. G., Holton, J. L., Revesz,

T., & Wood, N. W. (2005). A common LRRK2 mutation in idiopathic parkinson's disease. *The Lancet*, *365*(9457), 415–416. https://doi.org/10.1016/s0140-6736(05)17830-1

12. Benamer, H. T. S., & de Silva, R. (2010). LRRK2 G2019S in the North African population: A Review. *European Neurology*, *63*(6), 321–325. https://doi.org/10.1159/000279653

13. Taylor, M., & Alessi, D. R. (2020). Advances in elucidating the function of leucine-rich repeat protein kinase-2 in normal cells and Parkinson's disease. *Current Opinion in Cell Biology*, *63*, 102–113. https://doi.org/10.1016/j.ceb.2020.01.001

14. Zimprich, A., Biskup, S., Leitner, P., Lichtner, P., Farrer, M., Lincoln, S., Kachergus, J., Hulihan, M., Uitti, R. J., Calne, D. B., Stoessl, A. J., Pfeiffer, R. F., Patenge, N., Carbajal, I. C., Vieregge, P., Asmus, F., Müller-Myhsok, B., Dickson, D. W., Meitinger, T., Strom, T. M., Wszolek, Z. K., Gasser, T. (2004). Mutations in LRRK2 cause autosomal-dominant parkinsonism with pleomorphic pathology. *Neuron*, *44*(4), 601–607. https://doi.org/10.1016/j.neuron.2004.11.005

15. Wallings, R. L., & Tansey, M. G. (2019). LRRK2 regulation of immune-pathways and inflammatory disease. *Biochemical Society Transactions*, *47*(6), 1581–1595. https://doi.org/10.1042/bst20180463

16. Eguchi, T., Kuwahara, T., Sakurai, M., Komori, T., Fujimoto, T., Ito, G., Yoshimura, S.-ichiro, Harada, A., Fukuda, M., Koike, M., & Iwatsubo, T. (2018). LRRK2 and its substrate RAB GTPases are sequentially targeted onto stressed lysosomes and maintain their homeostasis. *Proceedings of the National Academy of Sciences*, *115*(39). https://doi.org/10.1073/pnas.1812196115

17. Henry, A. G., Aghamohammadzadeh, S., Samaroo, H., Chen, Y., Mou, K., Needle, E., & Hirst, W. D. (2015). Pathogenic LRRK2 mutations, through increased kinase activity, produce enlarged lysosomes with reduced degradative capacity and increase ATP13A2 expression. *Human Molecular Genetics*, *24*(21), 6013–6028. https://doi.org/10.1093/hmg/ddv314

18. Deniston, C. K., Salogiannis, J., Mathea, S., Snead, D. M., Lahiri, I., Matyszewski, M., Donosa, O., Watanabe, R., Böhning, J., Shiau, A. K., Knapp, S., Villa, E., Reck-Peterson, S. L., & Leschziner, A. E. (2020). Structure of LRRK2 in Parkinson’s disease and model for microtubule interaction. *Nature*, *588*(7837), 344–349. https://doi.org/10.1038/s41586-020-2673-2

19. Hui, K. Y., Fernandez-Hernandez, H., Hu, J., Schaffner, A., Pankratz, N., Hsu, N.-Y., Chuang, L.-S., Carmi, S., Villaverde, N., Li, X., Rivas, M., Levine, A. P., Bao, X., Labrias, P. R., Haritunians, T., Ruane, D., Gettler, K., Chen, E., Li, D., Schiff, E. R., Pontikos, N., Barzilai, N., Brant, S. R., Bressman, S., Cheifetz, A. S., Clark, L. N., Daly, M. J., Desnick, R. J., Duerr, R. H., Katz, S., Lencz, T., Myers, R. H., Ostrer, H., Ozelius,

L., Payami, H., Peter, Y., Rioux, J. D., Segal, A. W., Scott, W. K., Silverber, M. S., Vance, J. M., Ubarretxena-Belandia, I., Foroud, T., Atxmon, G., Pe'er, I., Ioannou, Y., McGovern, D. P. B., Yue, Z., Schadt, E. E., Cho, J. H., Peter, I. (2018). Functional variants in the LRRK2 gene confer shared effects on risk for Crohn's disease and Parkinson's disease. *Science Translational Medicine*, *10*(423). https://doi.org/10.1126/scitranslmed.aai7795

20. Fava, V. M., Xu, Y. Z., Lettre, G., Van Thuc, N., Orlova, M., Thai, V. H., Tao, S., Croteau, N., Eldeeb, M. A., MacDougall, E. J., Cambri, G., Lahiri, R., Adams, L., Fon, E. A., Trempe, J.-F., Cobat, A., Alcaïs, A., Abel, L., & Schurr, E. (2019). Pleiotropic effects for Parkin and LRRK2 in leprosy type-1 reactions and parkinson's disease. *Proceedings of the National Academy of Sciences*, *116*(31), 15616–15624. https://doi.org/10.1073/pnas.1901805116

21. Härtlova, A., Herbst, S., Peltier, J., Rodgers, A., Bilkei‐Gorzo, O., Fearns, A., Dill, B. D., Lee, H., Flynn, R., Cowley, S. A., Davies, P., Lewis, P. A., Ganley, I. G., Martinez, J., Alessi, D. R., Reith, A. D., Trost, M., & Gutierrez, M. G. (2018). LRRK2 is a negative regulator of mycobacterium tuberculosis phagosome maturation in macrophages. *The EMBO Journal*, *37*(12). https://doi.org/10.15252/embj.201798694

22. Ito, G., Okai, T., Fujino, G., Takeda, K., Ichijo, H., Katada, T., & Iwatsubo, T. (2007). GTP binding is essential to the protein kinase activity of LRRK2, a causative gene product for familial Parkinson's disease. *Biochemistry*, *46*(5), 1380–1388. https://doi.org/10.1021/bi061960m

23. Tomiyama, H., Li, Y., Funayama, M., Hasegawa, K., Yoshino, H., Kubo, S.-I., Sato, K., Hattori, T., Lu, C.-S., Inzelberg, R., Djaldetti, R., Melamed, E., Amouri, R., Gouider-Khouja, N., Hentati, F., Hatano, Y., Wang, M., Imamichi, Y., Mizoguchi, K., Miyajima, H., Obata, F., Toda, T., Farrer, M. J., Mizuno, Y., Hattori, N. (2006). Clinicogenetic study of mutations in LRRK2 exon 41 in Parkinson's disease patients from 18 countries. *Movement Disorders*, *21*(8), 1102–1108. https://doi.org/10.1002/mds.20886

24. Funayama, M., Hasegawa, K., Ohta, E., Kawashima, N., Komiyama, M., Kowa, H., Tsuji, S., & Obata, F. (2005). An LRRK2 mutation as a cause for the parkinsonism in the original park8 family. *Annals of Neurology*, *57*(6), 918–921. https://doi.org/10.1002/ana.20484

25. Schmidt, S. H., Knape, M. J., Boassa, D., Mumdey, N., Kornev, A. P., Ellisman, M. H., Taylor, S. S., & Herberg, F. W. (2019). The dynamic switch mechanism that leads to activation of LRRK2 is embedded in the dfgψ motif in the kinase domain. *Proceedings of the National Academy of Sciences*, *116*(30), 14979–14988. https://doi.org/10.1073/pnas.1900289116

26. Steger, M., Tonelli, F., Ito, G., Davies, P., Trost, M., Vetter, M., Wachter, S., Lorentzen, E., Duddy, G., Wilson, S., Baptista, M. A. S., Fiske, B. K., Fell, M. J., Morrow, J. A., Reith, A. D., Alessi, D. R., & Mann, M. (2016). Phosphoproteomics reveals that

parkinson's disease kinase LRRK2 regulates a subset of Rab GTPases. *ELife*, *5*. https://doi.org/10.7554/elife.12813

27. Simón-Sánchez, J., Martí-Massó, J.-F., Sánchez-Mut, J. V., Paisán-Ruiz, C., Martínez-Gil, A., Ruiz-Martínez, J., Sáenz, A., Singleton, A. B., López de Munain, A., & Pérez-Tur, J. (2006). Parkinson's disease due to the R1441G mutation in Dardarin: A founder effect in the Basques. *Movement Disorders*, *21*(11), 1954–1959. https://doi.org/10.1002/mds.21114

28. Gorostidi, A., Ruiz-Martínez, J., Lopez de Munain, A., Alzualde, A., & Martí Massó, J. F. (2008). LRRK2 G2019s and R1441G mutations associated with parkinson's disease are common in the Basque Country, but relative prevalence is determined by ethnicity. *Neurogenetics*, *10*(2), 157–159. https://doi.org/10.1007/s10048-008-0162-0

29. Nguyen, A. P., & Moore, D. J. (2017). Understanding the GTPase Activity of LRRK2: Regulation, Function, and Neurotoxicity. *Advances in neurobiology*, *14*, 71–88. https://doi.org/10.1007/978-3-319-49969-7_4

30. Haugarvoll, K., Rademakers, R., Kachergus, J. M., Nuytemans, K., Ross, O. A., Gibson, J. M., Tan, E.-K., Gaig, C., Tolosa, E., Goldwurm, S., Guidi, M., Riboldazzi, G., Brown, L., Walter, U., Benecke, R., Berg, D., Gasser, T., Theuns, J., Pals, P., Cras, P., De Deyn, P. P., Engelborghs, S., Pickut, B., Uitti, R. J., Forous, T., Nichols, W. C., Hagenah, J., Klein, C., Samii, A., Zabetian, C. P., Bonifati, V., Van Broeckhoven, C., Farrer, M. J., Wszolek, Z. K. (2008). LRRK2 R1441C parkinsonism is clinically similar to sporadic parkinson disease. *Neurology*, *70*(Issue 16, Part 2), 1456–1460. https://doi.org/10.1212/01.wnl.0000304044.22253.03

31. Lee, A. J., Wang, Y., Alcalay, R. N., Mejia-Santana, H., Saunders-Pullman, R., Bressman, S., Corvol, J.-C., Brice, A., Lesage, S., Mangone, G., Tolosa, E., Pont-Sunyer, C., Vilas, D., Schüle, B., Kausar, F., Foroud, T., Berg, D., Brockmann, K., Goldwurm, S., Siri, C., Asselta, R., Ruiz-Martinez, J., Mondragon, E., Marras, C., Ghate, T., Giladi, N., Mirelman, A.,Marder, K. (2017). Penetrance estimate of LRRK2 G2019S mutation in individuals of non-Ashkenazi jewish ancestry. *Movement Disorders*, *32*(10), 1432–1438. https://doi.org/10.1002/mds.27059

32. Sheng, Z., Zhang, S., Bustos, D., Kleinheinz, T., Le Pichon, C. E., Dominguez, S. L., Solanoy, H. O., Drummond, J., Zhang, X., Ding, X., Cai, F., Song, Q., Li, X., Yue, Z., van der Brug, M. P., Burdick, D. J., Gunzner-Toste, J., Chen, H., Liu, X., Estrada, A. A., Sweeney, Z. K., Scearce-Levie, K., Moffat, J. G., Kirkpatrick, D. S., Zhu, H. (2012). Ser1292 autophosphorylation is an indicator of LRRK2 kinase activity and contributes to the cellular effects of PD mutations. *Science Translational Medicine*, *4*(164). https://doi.org/10.1126/scitranslmed.3004485

33. Purlyte, E., Dhekne, H. S., Sarhan, A. R., Gomez, R., Lis, P., Wightman, M., Martinez, T. N., Tonelli, F., Pfeffer, S. R., & Alessi, D. R. (2017). Rab29 activation of the parkinson's disease‐associated LRRK2 kinase. *The EMBO Journal*, *37*(1), 1–18. https://doi.org/10.15252/embj.201798099

34. Dzamko, N., Deak, M., Hentati, F., Reith, A. D., Prescott, A. R., Alessi, D. R., & Nichols, R. J. (2010). Inhibition of LRRK2 kinase activity leads to dephosphorylation of Ser(910)/Ser(935), disruption of 14-3-3 binding and altered cytoplasmic localization. *The Biochemical journal*, *430*(3), 405–413. https://doi.org/10.1042/BJ20100784

35. Pellegrini, L., Wetzel, A., Grannó, S., Heaton, G., & Harvey, K. (2016). Back to the tubule: Microtubule dynamics in parkinson's disease. *Cellular and Molecular Life Sciences*, *74*(3), 409–434. https://doi.org/10.1007/s00018-016-2351-6

36. Berger, Z., Smith, K. A., & LaVoie, M. J. (2010). Membrane localization of LRRK2 is associated with increased formation of the highly active LRRK2 dimer and changes in its phosphorylation. *Biochemistry*, *49*(26), 5511–5523. https://doi.org/10.1021/bi100157u

37. Stormo, A. E. D., Shavarebi, F., FitzGibbon, M., Earley, E. M., Ahrendt, H., Lum, L. S., Verschueren, E., Swaney, D. L., Skibinski, G., Ravisankar, A., van Haren, J., Davis, E. J., Johnson, J. R., Von Dollen, J., Balen, C., Porath, J., Crosio, C., Mirescu, C., Iaccarino, C., Dauer, W. T., Nichols, J. R., Wittmann, T., Cox, T. C., Finkbeiner, S., Krogan, N. J., Oakes, S. A., Hiniker, A. (2022). The E3 ligase TRIM1 ubiquitinates LRRK2 and controls its localization, degradation, and toxicity. *Journal of Cell Biology*, *221*(4). https://doi.org/10.1083/jcb.202010065

38. Fuji, R. N., Flagella, M., Baca, M., S. Baptista, M. A., Brodbeck, J., Chan, B. K., Fiske, B. K., Honigberg, L., Jubb, A. M., Katavolos, P., Lee, D. W., Lewin-Koh, S.-C., Lin, T., Liu, X., Liu, S., Lyssikatos, J. P., O'Mahony, J., Reichelt, M., Roose-Girma, M., Sheng, Z., Sherer, T., Smith, A., Solon, M., Sweeney, Z. K., Tarrant, J., Urkowitz, A., Warming, S., Yaylaoglu, M., Shuo, Z., Zhu, H., Estrada, A. A., Watts, R. J. (2015). Effect of selective LRRK2 kinase inhibition on nonhuman primate lung. *Science Translational Medicine*, *7*(273). https://doi.org/10.1126/scitranslmed.aaa3634

39. Herzig, M. C., Kolly, C., Persohn, E., Theil, D., Schweizer, T., Hafner, T., Stemmelen, C., Troxler, T. J., Schmid, P., Danner, S., Schnell, C. R., Mueller, M., Kinzel, B., Grevot, A., Bolognani, F., Stirn, M., Kuhn, R. R., Kaupmann, K., van der Putten, P. H., Rovelli, G., Shimshek, D. R. (2011). LRRK2 protein levels are determined by kinase function and are crucial for kidney and lung homeostasis in mice. *Human Molecular Genetics*, *20*(21), 4209–4223. https://doi.org/10.1093/hmg/ddr348

40. Baptista, M. A. S., Merchant, K., Barrett, T., Bryce, D. K., Ellis, M., Estrada, A. A., Fell, M. J., Fiske, B. K., Fuji, R. N., Galatsis, P., Henry, A. G., Hill, S., Hirst, W., Houle, C., Kennedy, M. E., Liu, X., Maddess, M. L., Markgraf, C., Mei, H., Meier, W. A., Ploch, S. A., Royer, C. A., Rudolph, K. L., Sharma, A. K., Stepan, A. F., Steyn, S. J., Trost, C., Yin, Z., Yu, H. W., Wang, X. F., Sherer, T. B. (2018). LRRK2 kinase inhibitors induce a reversible effect in the lungs of non-human primates with no measurable pulmonary deficits. https://doi.org/10.1101/390815

41. Whiffin, N., Armean, I. M., Kleinman, A., Marshall, J. L., Minikel, E. V., Karczewski, K. J., Cummings, B. B., Francioli, L., Laricchia, K., Wang, Q., Guan, A., Alipanahi, B., Morrison, P., Baptista, M. A. S., Merchant, K. M., Ware, J. S., Havulinna, A. S., Iliadou, B., Lee, J., Nadkarni, G. N., Whiteman, C., Daly, M., Esko, T., Hultman, C. M., Ruth, J. F. L., Milani, L., Palotie, A., Pato, C. N., Pato, M. T., Saleheen, D., Sullivan, P. F., Alföldi, J., Cannon, P., MacArthur, D. G. (2019). Human loss-of-function variants suggest that partial LRRK2 inhibition is a safe therapeutic strategy for parkinson's disease. https://doi.org/10.1101/561472

42. Osanai, K., Higuchi, J., Oikawa, R., Kobayashi, M., Tsuchihara, K., Iguchi, M., Huang, J., Voelker, D. R., & Toga, H. (2010). Altered lung surfactant system in a rab38-deficient rat model of Hermansky-Pudlak syndrome. *American Journal of Physiology-Lung Cellular and Molecular Physiology*, *298*(2). https://doi.org/10.1152/ajplung.00242.2009

Chapter 2: TRIM1 regulates LRRK2 ubiquitination and localization

The TRIM superfamily of proteins is exceptionally large containing 70 proteins identified in humans, with many of them being linked to neuropsychiatric, developmental and cardiovascular disorders (1). For example, a genome-wide association study has shown that mutations to TRIM10, TRIM15, TRIM26, TRIM39 and TRIM40 are associated with multiple sclerosis risk (2). Loss of function mutations to the TRIM18/MID1 gene result in Opitz syndrome, a developmental disorder that causes midline defects (1). MID1 is a homolog of TRIM1 that shares 77% identity, and both have high expression in early development with MID1 playing a role in the regulation of gene expression in developing chick embryos and the development of the anterior cerebellar vermis in mice (3,4). Interestingly, TRIM1 shows high expression in the heart during development where MID1 is not expressed at all, meaning it may have an as-of-yet unknown role in development unique from MID1's (5). Similarly to LRRK2, these proteins are involved in a wide variety of cellular processes and more work needs to be done to better understand how their dysfunction results in pathogenesis (6).

This superfamily gets its name from its characteristic tripartite motif of a RING domain, one or two B-box domains and a Coiled-coil domain. Typically this motif is followed by a variable C-terminal region, with a PRY-SPRY protein-protein interaction domain being quite common, appearing in 60% of TRIM proteins (7). Most TRIM proteins are E3 ubiquitin ligases, made possible by their RING domain which binds to and activates E2 ubiquitin-conjugating enzymes, resulting in ubiquitination of the substrate (8).

E3 ligases can monoubiquitinate or polyubiquitinate in a chain with lysine linkages at ubiquitin lysines K6, K11, K27, K29, K33, K48 or K63. Variations in the chain and the lysines used affects the result of ubiquitination. For example, K48 linkages result in substrate

degradation by the proteasome whereas K63 linkages can perform various functions such as kinase activation (9). Proteasomal degradation is the most common result of ubiquitination by an E3 ligase (10). The B-box domain of TRIM proteins also contributes to E3 ligase activity and the Coiled-coil domain is a protein-protein interaction domain that allows for homomeric and heteromeric structures mediated by intertwining helices (11). TRIM protein subunit oligomerization is required for catalytic activity and polyubiquitin chain formation, likely through an allosteric mechanism which is not fully understood (12).

The TRIM1 gene is located within the PARK12 locus on the X-chromosome and mutations to this gene are found in a rare form of X-linked intellectual disability, pointing to the importance of TRIM1 in the brain (13, 14). Despite its importance, TRIM1 is a relatively understudied protein and not much is understood about its function beyond its E3 ligase activity. Our interest in TRIM1 stems from work in our lab that used an affinity purification-MS assay to reveal 48 novel LRRK2 binding partners, with TRIM1 being the strongest result. Subsequent immunoprecipitation assays confirmed that TRIM1 does indeed bind to LRRK2, necessitating research into TRIM1-LRRK2 interaction. To determine the rough location at which these two proteins interact, truncated mutants of both TRIM1 and LRRK2 were used in coimmunoprecipitation experiments. These showed that TRIM1 binds with its B-box domains between the Ankyrin and Leucine Rich Repeat domains of LRRK2 (15).

Our lab has also shown that TRIM1 is able to ubiquitinate LRRK2, and this finding will be explored further in the results section. With this knowledge, other members of our lab used mass spectrometry and flow cytometry to determine the effect of TRIM1 mediated LRRK2 ubiquitination. Understanding the specifics of the polyubiquitin chain on LRRK2 is important to understanding its effects, and thus MS targeting the ubiquitin protein on LRRK2

immunoprecipitation samples was performed in HEK-293T cells. K48 linkages were detected by MS in the presence of TRIM1, while no polyubiquitin linkages were detected in any other samples. Additionally, the K48 signal was greatly enriched in the presence of the MG132 proteasome inhibitor. This paired with the fact that polyubiquitination at K48 is known to target proteins to the proteasome indicates that TRIM1 ubiquitination of LRRK2 directs it to the proteasome for degradation (16). It is also important to note that TRIM1 mediated LRRK2 degradation was observed by our lab in primary cortical neurons, pointing to the TRIM1-LRRK2 interaction potentially being relevant to PD (15).

Materials and Methods

Cell culture

All cells were grown at 37°C and 5% CO_2 in a humidified incubator. H1299 cells used in microscopy were grown in RPMI 1640 supplemented with 10% FBS, 25mM HEPES and 2.0 g/L NaHCO3. HEK293T cells were grown in DMEM supplemented with 10% FBS. PC12 cells used in neurite outgrowth studies were cultured in DMEM with 15% tet-free FBS and 2mM GlutaMAX, while the dox-inducible LRRK2 PC12 line was grown in DMEM with 10% horse serum and 5% tet-free FBS or DMEM with 15% tet-free FBS, 2mM GlutaMAX and selection reagents: 400ug/ml Geneticin and 200ug/ml hygromycin. They were differentiated in DMEM with 1% horse serum and 100ng/ml neurite growth factor, which was replaced every 48 hours.

Plasmids and Transfection

GFP-LRRK2 and FLAG-myc-LRRK2 were expressed in the pcDNA5 frt/to vector. TRIM1, TRIM1ΔRF and TRIM18 were expressed in the pCMV-C2-6myc or pCMV-C2-EGFP vectors. The mCherry-tubulin plasmid was gifted by Roger Tsien and the prk5-HA-ubiquitin

plasmid was gifted by Tim Dawson. Transfection into HEK293T cells was performed with either Lipofectamine 2000 (Thermo Fisher Scientific) or Lipofectamine LTX (Thermo Fisher Scientific). H1299 cells were transfected with Lipofectamine 2000 and PC 12 cells were transfected with Lipofectamine 3000 or Lipofectamine LTX. Transfection procedure was carried out in accordance with manufacturer protocol.

Microscopy & Imaging - LRRK2 Microtubule Binding

H1299 Cells were plated on 35mm poly-D-lysine coated coverslip dishes (MatTek, P35GC-0-14-C), with 4×10^5 cells on each dish. 24 hours post-transfection, the cells were imaged using an Olympus Fluoview 1000 laser scanning confocal microscope or a Nikon Eclipse ti fluorescence microscope with a 60x oil-immersion objective. Because this process was done with live cells, microscopy and imaging was performed with temperature and CO_2 control at 37°C and 5% CO_2. Only doubly-transfected cells with green and red fluorescence were counted, if TRIM1 or tubulin showed microtubule localization. The operator was blinded to conditions and took 50 images per plate, with 2 plates per condition. Each experiment had 3 replicates, and the percentage of cells with microtubule-localized LRRK2 was calculated, with the error expressed as the standard deviation. Additionally, the Fiji image processing package was used to process the microscopy images afterward.

Neurite Outgrowth Assay

The dox-inducible LRRK2 G2019S PC12 line was seeded in a 96 well plate at 20,000 cells/well. They were then transfected with 30ng/well of pMax-GFP and 200ng/well of either mCherry-TRIM1 or an empty mCherry vector. 24 hours post-transfection, the cells were transferred to 35mm poly-D-lysine coated coverslips (Neuvitro) with and without dox-induction of LRRK2-G2019S at 1ug/ml. Cells were differentiated as described, then after 5 days they were

fixed using 4% PFA in PBS for 20 minutes. This was followed by 3 PBS washes, then a 1 hour permeabilization step using PBS with 10% goat serum, 0.4% Triton X-100, 30 mg/ml BSA and 10 mg/ml glycine. Then after 3 PBS washes, the coverslips were mounted on slides with Vectashield hardmount. Microscopy and imaging was carried out using a Keyence BZ-X700 fluorescence microscope with a 40x objective. Only cells with both fluorescence signals were imaged and counted. The analysis of neurite outgrowth presence and length was performed in the ImageJ image processing program.

Cell Lysis

Scraping was used to detach adherent cells, which were then pelleted at 270 RCF and cleared of any residual media by washing twice with PBS. Then cells were resuspended in ice-cold lysis buffer comprised of 50 mM Tris, pH 7.5, 150 mM NaCl, 1 mM EDTA, and 0.5% NP-40 supplemented with Phosstop phosphatase inhibitor (Roche, 04906845001)) and cOmplete protease inhibitor (Roche, 11836170001). The resuspension was then left on a rotator for 30 minutes at 4°C. After lysis, the solution was centrifuged at >10,000 RCF for 5 minutes at 4°C to clear cell debris. The supernatant was separated and its protein concentration was determined with the Pierce BCA Protein Assay Kit (Thermo Fisher Scientific, 23225). Protein concentrations were normalized across samples, which were then ready for immunoprecipitation or for immunoblotting following addition of 4× NuPAGE LDS loading buffer (Invitrogen, NP0007) supplemented with 5% β-mercaptoethanol.

Immunoprecipitation

After normalization of protein concentration, 20-40µl of antibody-beads were added to bind tagged proteins. In the ubiquitination assay, myc-trap_A and magnetic myc-trap_MA (Chromotek) were used to bind myc-TRIM1 and myc-CHIP. The solution was incubated at 4°C

for 2-12 hours, after which the beads underwent 3 washes with a wash buffer comprised of 50 mM Tris, pH 7.5, 150–500 mM NaCl, and 1 mM EDTA. Then protein was eluted off of the beads by a 70–95°C incubation in a small volume (40–80 µl) of 4× NuPAGE LDS loading buffer supplemented with 5% β-mercaptoethanol.

Immunoblotting

NuPage 4-12% Bis-Tris (Invitrogen, NP0321) and/or 3-8% Tris-acetate (Invitrogen, EA0375) gels were used to run samples, with Tris-acetate being preferentially used for the high molecular weight protein LRRK2. After running, the gels were transferred onto PVDF membranes (EMD Millipore, IPFL00010) with the Genscript eBlot L1 transfer system. Membranes were blocked with Intercept TBS blocking buffer (LI-COR, 927-60001) for 30 minutes. The primary antibodies used were: mouse anti-LRRK2 N241 (Neuromab, 75-253), rabbit anti-LRRK2 C41-2 (Abcam, ab133474), rabbit anti-FLAG (Sigma-Aldrich, F7425), mouse anti-myc (clone 9E10, Sigma-Aldrich, M4439), rabbit anti-myc (clone 71D10, Cell Signaling, 2278), rabbit anti-mCherry (Abcam, ab167453), rabbit anti-TRIM1 (M2448; Sigma-Aldrich), mouse anti-GFP (clone GF28R, Thermo Fisher Scientific, MA5-15256), rabbit anti-HA (clone C29F4, Cell Signaling, 3724S), mouse anti-HA (Sigma-Aldrich, H3663), mouse anti-ubiquitin (Millipore Sigma, MAB1510-I) rabbit anti-actin (Cell Signaling, clone 13E5, 4970), mouse anti-actin (Cell Signaling, clone 8H10D10, 3700S) and rabbit anti-tubulin (Cell Signaling, 15115S). All primary antibodies were diluted 1:1000, except for the actin and tubulin antibodies which were diluted at 1:2000 and 1:5000 respectively. Membranes were incubated in primary for either 3 hours at room temperature or overnight at 4°C. The secondary antibodies, IRDye 800CW goat anti-mouse (LI-COR, 926-32210) and 680RD goat anti-rabbit (LI-COR, 926-68071) were diluted 1:10,000 and incubated for 30 minutes at room temperature. The

LI-COR Odyssey CLx system was used to image and quantify fluorescence, which was then interpreted using Image Studio acquisition software.

Results

TRIM1 controls LRRK2 microtubule localization.

It was previously mentioned that TRIM proteins contain a C-terminal variable region. Within TRIM1's variable region is a COS domain, which has been shown to be responsible for microtubule localization of TRIM1 and other proteins (17). On the other hand, the majority of wildtype LRRK2 localizes diffusely throughout the cytoplasm. Although, there are a handful of pathogenic LRRK2 mutations (R1441C, R1441G, Y1699C, I2020T) which increase LRRK2's otherwise very sparse microtubule localization (18).

To investigate the effect of TRIM1 on LRRK2 localization, I overexpressed mCherry-TRIM1 and GFP-LRRK2 into H1299 cells, which are human lung cancer cells. H1299 cells were chosen because they are very large and flat, allowing for enhanced visibility of the microtubule structure by live-cell confocal microscopy. First, I confirmed that GFP-LRRK2 was spread diffusely throughout the cytoplasm and that mCherry-TRIM1 localized to the microtubules as expected (5, 18). With that established, I performed a co-transfection of GFP-LRRK2 with mCherry-TRIM1 and found that TRIM1 has a strong regulatory effect on LRRK2 subcellular localization (Fig. 1a). Upon coexpression, nearly every single cell expressing both proteins had GFP-LRRK2 and mCherry-TRIM1 localized to the microtubules (99% ± 1%; Fig. 1b). Additionally, a control condition of GFP-LRRK2 coexpression with mCherry-tubulin, which marks microtubules but should not affect LRRK2 localization, resulted in the expected sparse microtubule localization of GFP-LRRK2 (6% ± 2%, Fig. 1b).

To test whether the ability to regulate LRRK2 microtubule localization is specific to TRIM1, we performed similar coexpression experiments using the TRIM1 homolog TRIM18, TRIM1's closest relative which shares 77% identity. When mCherry-TRIM18 was expressed, GFP-LRRK2 was not recruited to the microtubules (3% ± 3%, Fig. 1b) indicating this interaction is unique to TRIM1. Finally, to test whether TRIM1 E3 ligase activity is required for microtubule localization we performed the same experiment using the GFP tagged RING finger deleted TRIM1 mutant (TRIM1ΔRF), which abolishes E3 ligase activity, and found that it had no effect on mCherry-LRRK2 microtubule localization (99% ± 1%, Fig. 1b).

TRIM1 ubiquitinates LRRK2.

As mentioned before, most TRIM proteins are E3 ubiquitin ligases and TRIM1 is no different. TRIM1's E3 ligase activity allows it to transfer the regulatory protein ubiquitin onto other proteins, which typically marks the target protein for degradation. Therefore, we wanted to test if TRIM1 is able to ubiquitinate LRRK2 and potentially regulate LRRK2 degradation. Coexpression of HA-ubiquitin, myc-TRIM1 and FLAG-LRRK2 followed by in vivo ubiquitination assays showed that TRIM1 does ubiquitinate LRRK2. The positive control used myc-CHIP, a protein known to ubiquitinate LRRK2, and the negative control used HA-ubiquitin with no E3 ubiquitin ligase transfection (19). To test if TRIM1 affects LRRK2 turnover, we coexpressed myc-TRIM1 with FLAG-LRRK2 and found on a western blot timecourse that TRIM1 expression results in decreased LRRK2 levels compared to an empty vector. Work by others in our lab using flow cytometry substantiated this result. Further, they showed that TRIM1ΔRF does not result in LRRK2 degradation, indicating that ubiquitination of LRRK2 by TRIM1 is responsible for the observed LRRK2 turnover.

TRIM1 is protective against the LRRK2-G2019S mediated neurite outgrowth defect.

Neurites are projections extending out from developing neurons which ultimately become dendrites or axons. The neurite outgrowth process is dependent on microtubules and it has been shown that the LRRK2-G2019S mutation disrupts this process (20). In prior experiments, we have found that type 1 LRRK2 kinase inhibitors reversed the LRRK2-G2019S neurite outgrowth defect (15). Therefore we speculated that due to TRIM1's role in regulating LRRK2 localization and degradation, overexpression of TRIM1 may similarly reverse the observed defect in neuronal cells.

We performed this experiment in rat PC12 pheochromocytoma cells with dox-inducible LRRK2-G2019S. The cells were transfected with mCherry-TRIM1 or an empty control vector, with and without dox induction, followed by a 5 day treatment with nerve growth factor to stimulate neurite outgrowth. We then imaged the cells and neurite length as well as the proportion of cells with a neurite at least as long as the cell body was quantified (Fig. 3b and 3c). Firstly, TRIM1 overexpression did not affect neurite outgrowth prevalence (46% ± 9% had neurites with TRIM1 overexpression compared to 49% ± 2% with empty vector). As expected, dox-induced LRRK2-G2019S expression greatly reduced neurite outgrowth (29% ± 6% had neurites with LRRK2-G2019S overexpression). However, upon coexpression with TRIM1 the proportion of cells with neurites returned to normal (44% ± 6% with TRIM1 and LRRK2-G2019S coexpression). Similar results were observed when measuring neurite length (Fig. 3c). TRIM1 overexpression alone did not affect neurite length (46.1 ± 8.5μm in TRIM1 transfected cells compared to 40.8 ± 3.9μm with empty vector). Dox-induction of LRRK2-G2019S reduced neurite length significantly (32.4 ± 3.5μm), an effect that was not observed upon coexpression with TRIM1 (48.7 ± 7.5μm). This provides an interesting example

of a LRRK2 regulator directly protecting against a known neurodegenerative effect of a pathogenic LRRK2 mutant.

TRIM1 mutants identified in intellectual disability show abnormal localization.

Historical data has shown the TRIM1 R347G mutant to be responsible for the X-linked intellectual disability (ID) shared among several members of a large Indian family (21). The R347G mutant leads to loss of function (LoF) in the COS domain. Building on this, work done by our collaborators identified 7 additional and very rare TRIM1 variants that were found in patients with similar ID. 4 were LoF mutations (W455*, E428Gfs*34, S483Qfs*2 and F692Lfs*8) and 3 were missense mutations (G520S, W487C and R347Q). The small group of 10 subjects with these mutations were all male and showed mild to severe ID. They also suffered from a number of other conditions including autism spectrum disorder, ADHD and epilepsy.

To investigate the pathogenic disruptions to TRIM1 function caused by these mutations, I performed confocal fluorescence microscopy focusing on intracellular localization. I found that the mutants did show deviations from typical TRIM1 microtubule localization (Fig. 4). The LoF mutations showed no microtubule localization, instead forming large and abnormal perinuclear aggregates. The missense mutations still had partial microtubule localization along with the abnormal aggregates. Similarly, LRRK2 did not localize to the microtubules and was instead recruited to these abnormal aggregates, which likely had effects on LRRK2 function which we have not delineated. This disruption to typical TRIM1 localization is likely one of the driving factors behind the observed ID and other conditions. These findings also provide additional support for the importance of TRIM1 in the brain. Thus, our findings regarding its interactions with LRRK2 may be worth studying in the context of PD.

Discussion

This work has shown TRIM1 to be a novel regulator of LRRK2, with control over its localization and degradation. TRIM1 reliably recruits LRRK2 to the microtubules, where it ubiquitinates LRRK2 to drive its degradation. We have also shown that TRIM1 is protective against the neurite outgrowth defect caused by the pathogenic G2019S LRRK2 mutation.

I showed by fluorescence microscopy that TRIM1 coexpression consistently results in LRRK2 microtubule localization. By the same methods, I also showed that this interaction seems to be specific to the TRIM1 protein and that ubiquitination is not required for LRRK2 recruitment. Previous research has clearly shown that LRRK2 can be found at the microtubules, however it is still unclear what the function of microtubule-bound LRRK2 is. With these findings, we have uncovered the microtubule cytoskeleton as an important region in the study of LRRK2 degradation.

Furthermore, our lab has uncovered an interesting dynamic between TRIM1 and 14-3-3 via phosphorylation of pS910 and pS935 of LRRK2. Phosphorylation of LRRK2's regulatory loop region near the TRIM1 binding site, including the S910 and S935 sites, influences LRRK2's binding to either TRIM1 or 14-3-3, with TRIM1 preferentially binding to unphosphorylated LRRK2 (15). The 14-3-3 protein regulates LRRK2 localization and is intimately tied to LRRK2 kinase activity, primarily because it keeps LRRK2 in the cytoplasm and away from membranes where its activity is typically elevated. Additionally, the 14-3-3 protein has clinical relevance to PD evidenced by reduced LRRK2 binding to 14-3-3 in neurons of the Substantia Nigra in PD patients (22). Therefore, TRIM1 's competitive relationship with 14-3-3 could be important. This necessitates further research into the downstream effects of TRIM1-LRRK2 interaction, especially regarding the physiological function of microtubule-bound LRRK2.

We have also shown that TRIM1 ubiquitinates LRRK2, driving LRRK2 degradation. Further work done by others in our lab has shown that TRIM1-driven polyubiquitin chains with K48 linkages target LRRK2 for proteasomal degradation. Given that increased LRRK2 kinase activity is typically the driving force behind LRRK2-PD pathogenesis, TRIM1's role in LRRK2 turnover could have clinical relevance. This is supported by our finding that TRIM1 is protective against the LRRK2 G2019S driven neurite outgrowth defect.

A shortcoming of these experiments which could be addressed in the future is that all microscopy experiments relied on the overexpression of LRRK2. Due to LRRK2's low expression levels, endogenous LRRK2 can be quite challenging to study with many experimental techniques. Using a number of techniques including ice-cold ethanol incubation after PFA fixation and interferon gamma treatment, I have been unable to obtain a satisfactory endogenous LRRK2 signal by immunofluorescence in my research. However, others have been able to visualize endogenous LRRK2 in certain cell types (23). Replicating these results under physiological conditions with endogenous LRRK2 would help to further solidify these findings.

Figure 2.1: TRIM1 coexpression regulates LRRK2 microtubule localization. (A) Confocal microscopy imaging showing an H1299 cell expressing fluorescently-tagged protein. The top shows GFP-LRRK2 (left), mCherry-tubulin (middle) and an overlaid image (right). The bottom shows GFP-LRRK2 (left), mCherry-TRIM1 (middle) and an overlaid image (right). Scale bar = 10μm. (B) Quantification of the percentage of H1299 cells with microtubule-localized LRRK2 with coexpression of (left to right): mCherry-tubulin, mCherry-TRIM1, mCherry-TRIM18 and mCherry-TRIM1ΔRF. The percentage of cells with microtubule associated LRRK2 was 6% ± 2% with mCh-tubulin, 99% ± 1% with mCh-TRIM1, 3% ± 3% with mCh-TRIM18 and 99% ± 1% with mCh-TRIM1ΔRF.

Figure 2.1

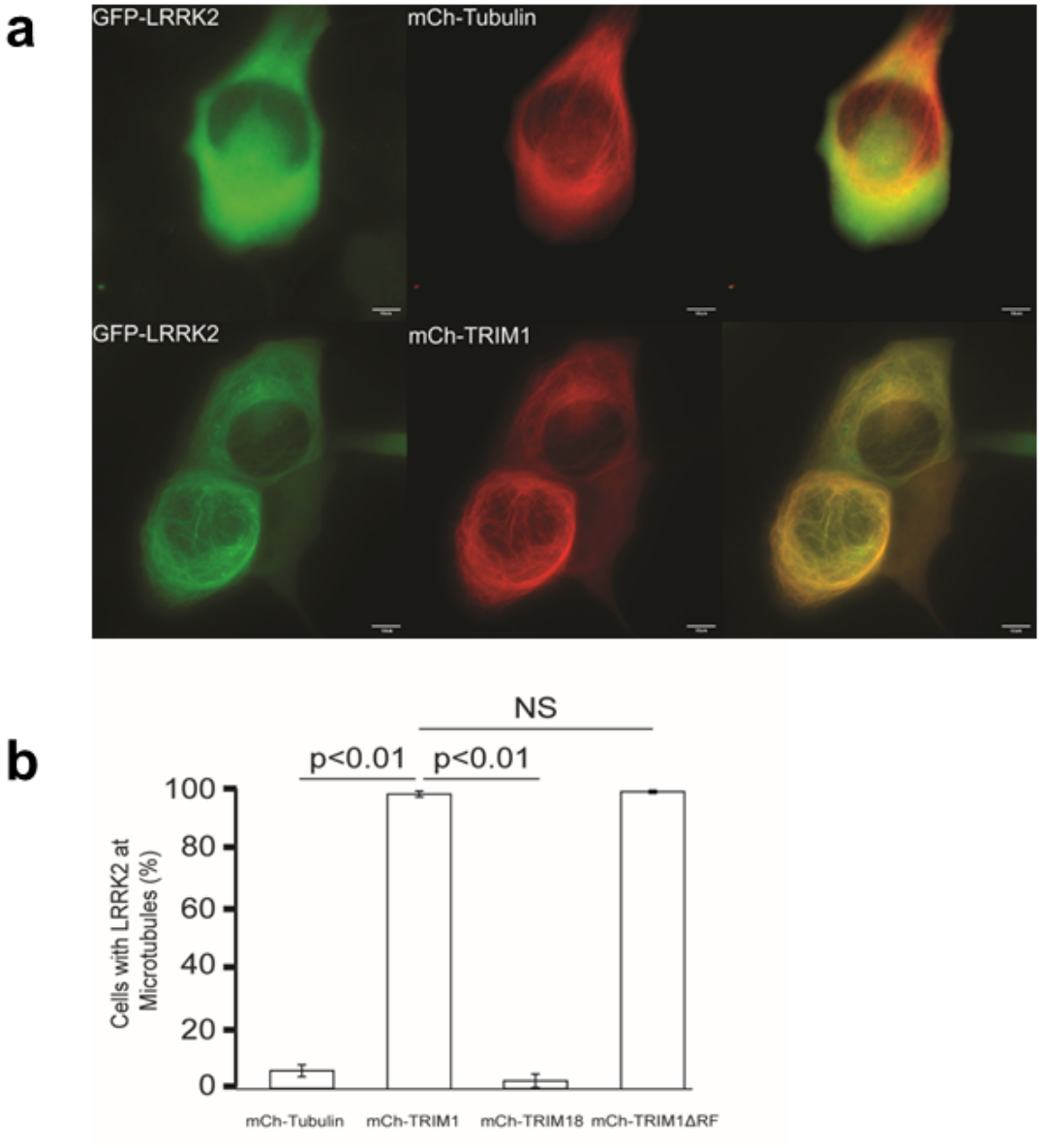
a
GFP-LRRK2
mCh-Tubulin
GFP-LRRK2
mCh-TRIM1
b
NS
p<0.01
p<0.01
Cells with LRRK2 at Microtubules (%)
100
80
60
40
20
0
mCh-Tubulin
mCh-TRIM1
mCh-TRIM18
mCh-TRIM1ΔRF

Figure 2.2: TRIM1 ubiquitinates LRRK2 and triggers its degradation. (A) Stormo et al. 2022, Figure 3a. (Top) Immunoprecipitation of GFP-LRRK2, also recovering HA-ubiquitin. GFP-LRRK2 and HA-ubiquitin are present in all samples. The first lane has no additional overexpression, the second lane contains overexpressed myc-TRIM1-WT and the fourth lane contains overexpressed myc-TRIM1-ΔRF. (Bottom) The input displayed with the same layout (B) Stormo et al. 2022, Figure S2a. Immunoblot of FLAG-LRRK2 degradation upon cotransfection with myc-TRIM1 compared to empty vector control. Coexpression of FLAG-LRRK2 with the empty vector (left) shows higher LRRK2 levels than coexpression with myc-TRIM1 (right).

Figure 2.3: TRIM1 is protective against LRRK2-G2019S mediated neurite outgrowth defect. (A) Stormo et al. 2022, Figure 9d. Rat PC12 cells with dox-inducible GFP-LRRK2 G2019S. The top shows empty vector (left) and overexpressed mCherry-TRIM1 (right). The bottom shows coexpression of empty vector with dox-induced GFP-LRRK2 G2019S (left) and coexpression of mCherry-TRIM1 with dox-induced GFP-LRRK2 G2019S (right). Scale bar = 10μm. TRIM1 coexpression recovers normal neurite morphology. (B) Stormo et al. 2022, Figure 9e. Quantification of the percentage of rat PC12 cells with neurites at least as long as the cell body under protein overexpression. Neurites were present in 49% ± 2% with empty vector, 29% ± 6% with LRRK2-G2019S, 46% ± 9% with TRIM1 and 44% ± 6% with TRIM1 and LRRK2-G2019S coexpression. (C) Stormo et al. 2022, Figure 9f. Quantification of neurite length in rat PC12 cells with protein overexpression. Neurites were 40.8 ± 3.9μm with empty vector, 46.1 ± 8.5μm with TRIM1, 32.4 ± 3.5μm with LRRK2-G2019S and 48.7 ± 7.5μm with coexpression of LRRK2-G2019S and TRIM1.

Stormo, A. E. D., Shavarebi, F., FitzGibbon, M., Earley, E. M., Ahrendt, H., Lum, L. S., Verschueren, E., Swaney, D. L., Skibinski, G., Ravisankar, A., van Haren, J., Davis, E. J., Johnson, J. R., Von Dollen, J., Balen, C., Porath, J., Crosio, C., Mirescu, C., Iaccarino, C., Dauer, W. T., Nichols, J. R., Wittmann, T., Cox, T. C., Finkbeiner, S., Krogan, N. J., Oakes, S. A., Hiniker, A. (2022). The E3 ligase TRIM1 ubiquitinates LRRK2 and controls its localization, degradation, and toxicity. *Journal of Cell Biology*, *221*(4). https://doi.org/10.1083/jcb.202010065

Figure 2.4: TRIM1 mutants identified in intellectual disability show abnormal localization. Each set of 3 images shows one cell with GFP-TRIM1 (left), mCh-LRRK2 (middle) and an overlaid image (right). The left side shows (top to bottom) wildtype MID2 (TRIM1) and mutants W455*, E428Gfs*34 and S483Qfs*2. The right side shows (top to bottom) mutants F692Lfs*8, G520S, W487C and R347Q. The scale bar is 10μm.

Figure 2.4

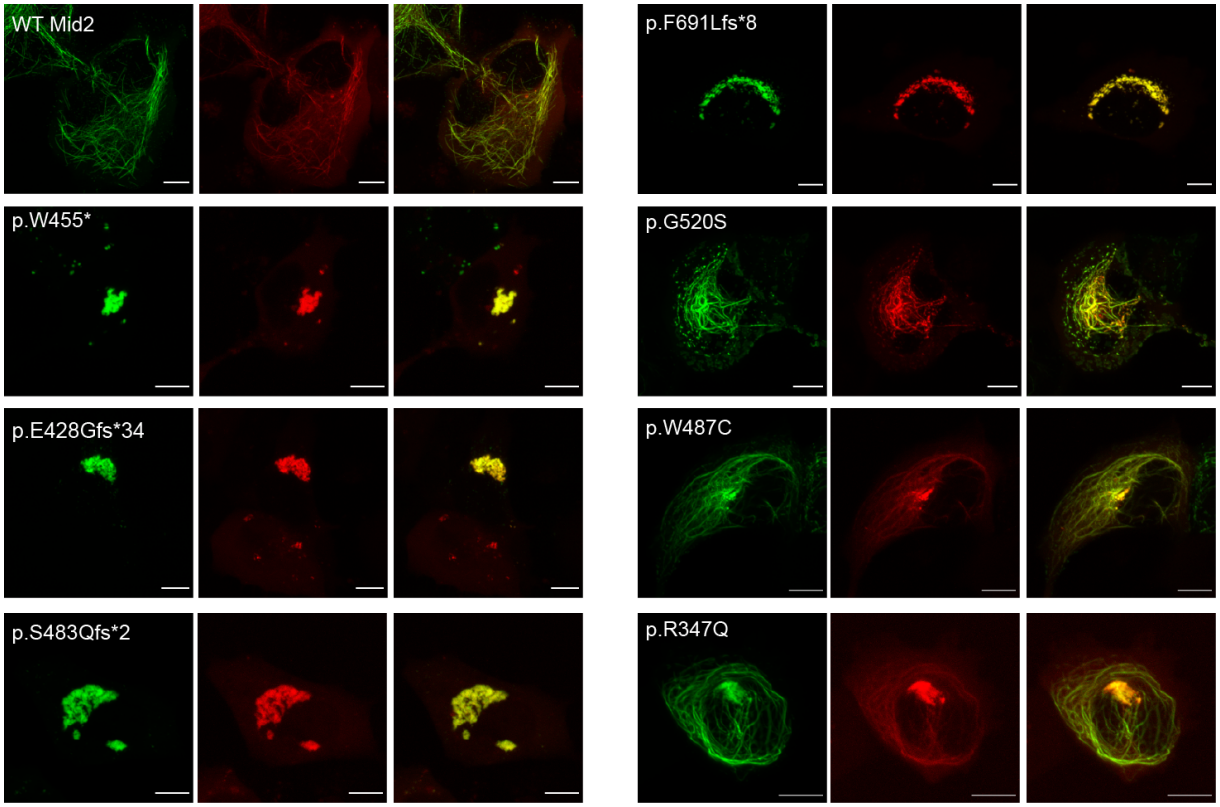
WT Mid2
p.F691Lfs*8
p.W455*
p.G520S
p.E428Gfs*34
p.W487C
p.S483Qfs*2
p.R347Q

References

1. Watanabe, M., & Hatakeyama, S. (2017). Trim proteins and diseases. *Journal of Biochemistry*. https://doi.org/10.1093/jb/mvw087

2. Baranzini, S. E., Wang, J., Gibson, R. A., Galwey, N., Naegelin, Y., Barkhof, F., Radue, E.-W., Lindberg, R. L. P., Uitdehaag, B. M. G., Johnson, M. R., Angelakopoulou, A., Hall, L., Richardson, J. C., Prinjha, R. K., Gass, A., Geurts, J. J. G., Kragt, J., Sombekke, M., Vrenken, H., Qualley, P., Lincoln, R. R., Gomez, R., Caillier, S. J., George, M. F., Mousavi, H., Guerrero, R., Okuda, D. T., Cree, B. A. C, Green, A. J., Waubant, E., Goodin, D. S., Pelletier, D., Matthews, P. M., Hauser, S. L., Kappos, L., Polman, C. H., Oksenberg, J. R. (2008). Genome-wide association analysis of susceptibility and clinical phenotype in multiple sclerosis. *Human Molecular Genetics*, *18*(4), 767–778. https://doi.org/10.1093/hmg/ddn388

3. Granata, A., & Quaderi, N. A. (2003). The opitz syndrome gene mid1 is essential for establishing asymmetric gene expression in Hensen's node. *Developmental Biology*, *258*(2), 397–405. https://doi.org/10.1016/s0012-1606(03)00131-3

4. Lancioni, A., Pizzo, M., Fontanella, B., Ferrentino, R., Napolitano, L. M., De Leonibus, E., & Meroni, G. (2010). Lack of Mid1, the mouse ortholog of the Opitz syndrome gene, causes abnormal development of the anterior cerebellar vermis. *The Journal of Neuroscience*, *30*(8), 2880–2887. https://doi.org/10.1523/jneurosci.4196-09.2010

5. Buchner, G., Montini, E., Andolfi, G., Quaderi, N., Cainarca, S., Messali, S., Bassi, M. T., Ballabio, A., Meroni, G., & Franco, B. (1999). Mid2, a homologue of the Opitz syndrome gene MID1: Similarities in subcellular localization and differences in expression during development. *Human Molecular Genetics*, *8*(8), 1397–1407. https://doi.org/10.1093/hmg/8.8.1397

6. Meroni, G. (2012). Genomics and evolution of The trim gene family. *Advances in Experimental Medicine and Biology*, 1–9. https://doi.org/10.1007/978-1-4614-5398-7_1

7. García-Sastre, A., & Miorin, L. (2016). Intrinsic cellular defenses (TRIMS) in modulating viral infection and immunity. *Encyclopedia of Immunobiology*, 235–242. https://doi.org/10.1016/b978-0-12-374279-7.14004-4

8. Deshaies, R. J., & Joazeiro, C. A. P. (2009). RING domain E3 ubiquitin ligases. *Annual Review of Biochemistry*, *78*(1), 399–434. https://doi.org/10.1146/annurev.biochem.78.101807.093809

9. Chen, Z. J., & Sun, L. J. (2009). Nonproteolytic functions of Ubiquitin in cell signaling. *Molecular Cell*, *33*(3), 275–286. https://doi.org/10.1016/j.molcel.2009.01.014

10. Nandi, D., Tahiliani, P., Kumar, A., & Chandu, D. (2006). The Ubiquitin-Proteasome System. *Journal of Biosciences*, *31*(1), 137–155. https://doi.org/10.1007/bf02705243

11. Li, Y., Wu, H., Wu, W., Zhuo, W., Liu, W., Zhang, Y., Cheng, M., Chen, Y.-G., Gao, N., Yu, H., Wang, L., Li, W., & Yang, M. (2014). Structural insights into the trim family of Ubiquitin E3 ligases. *Cell Research*, *24*(6), 762–765. https://doi.org/10.1038/cr.2014.46

12. Streich, F. C., Ronchi, V. P., Connick, J. P., & Haas, A. L. (2013). Tripartite motif ligases catalyze polyubiquitin chain formation through a cooperative allosteric mechanism. *Journal of Biological Chemistry*, *288*(12), 8209–8221. https://doi.org/10.1074/jbc.m113.451567

13. Pankratz, N. (2003). Genome-wide linkage analysis and evidence of gene-by-gene interactions in a sample of 362 multiplex parkinson disease families. *Human Molecular Genetics*, *12*(20), 2599–2608. https://doi.org/10.1093/hmg/ddg270

14. Geetha, T. S., Michealraj, K. A., Kabra, M., Kaur, G., Juyal, R. C., & Thelma, B. K. (2013). Targeted deep resequencing identifies Mid2 mutation for X-linked intellectual disability with varied disease severity in a large kindred from India. *Human Mutation*, *35*(1), 41–44. https://doi.org/10.1002/humu.22453

15. Stormo, A. E. D., Shavarebi, F., FitzGibbon, M., Earley, E. M., Ahrendt, H., Lum, L. S., Verschueren, E., Swaney, D. L., Skibinski, G., Ravisankar, A., van Haren, J., Davis, E. J., Johnson, J. R., Von Dollen, J., Balen, C., Porath, J., Crosio, C., Mirescu, C., Iaccarino, C., Dauer, W. T., Nichols, J. R., Wittmann, T., Cox, T. C., Finkbeiner, S., Krogan, N. J., Oakes, S. A., Hiniker, A. (2022). The E3 ligase TRIM1 ubiquitinates LRRK2 and controls its localization, degradation, and toxicity. *Journal of Cell Biology*, *221*(4). https://doi.org/10.1083/jcb.202010065

16. Wang, G., Gao, Y., Li, L., Jin, G., Cai, Z., Chao, J.-I., & Lin, H.-K. (2012). K63-linked ubiquitination in kinase activation and cancer. *Frontiers in Oncology*, *2*. https://doi.org/10.3389/fonc.2012.00005

17. Short, K. M., & Cox, T. C. (2006). Subclassification of the RBCC/trim superfamily reveals a novel motif necessary for microtubule binding. *Journal of Biological Chemistry*, *281*(13), 8970–8980. https://doi.org/10.1074/jbc.m512755200

18. Kett, L. R., Boassa, D., Ho, C. C.-Y., Rideout, H. J., Hu, J., Terada, M., Ellisman, M., & Dauer, W. T. (2011). LRRK2 Parkinson disease mutations enhance its microtubule association. *Human Molecular Genetics*, *21*(4), 890–899. https://doi.org/10.1093/hmg/ddr526

19. Ko, H. S., Bailey, R., Smith, W. W., Liu, Z., Shin, J.-H., Lee, Y.-I., Zhang, Y.-J., Jiang, H., Ross, C. A., Moore, D. J., Patterson, C., Petrucelli, L., Dawson, T. M., & Dawson, V. L. (2009). Chip regulates leucine-rich repeat kinase-2 ubiquitination, degradation, and toxicity. *Proceedings of the National Academy of Sciences*, *106*(8), 2897–2902. https://doi.org/10.1073/pnas.0810123106

20. MacLeod, D., Dowman, J., Hammond, R., Leete, T., Inoue, K., & Abeliovich, A. (2006). The familial parkinsonism gene LRRK2 regulates neurite process morphology. *Neuron*, *52*(4), 587–593. https://doi.org/10.1016/j.neuron.2006.10.008

21. Geetha, T. S., Michealraj, K. A., Kabra, M., Kaur, G., Juyal, R. C., & Thelma, B. K. (2013). Targeted deep resequencing identifies MID2 mutation for X-linked intellectual disability with varied disease severity in a large kindred from India. *Human Mutation*, *35*(1), 41–44. https://doi.org/10.1002/humu.22453

22. Di Maio, R., Hoffman, E. K., Rocha, E. M., Keeney, M. T., Sanders, L. H., De Miranda, B. R., Zharikov, A., Van Laar, A., Stepan, A. F., Lanz, T. A., Kofler, J. K., Burton, E. A., Alessi, D. R., Hastings, T. G., & Greenamyre, J. T. (2018). LRRK2 activation in idiopathic parkinson's disease. *Science Translational Medicine*, *10*(451). https://doi.org/10.1126/scitranslmed.aar5429

23. Eguchi, T., Kuwahara, T., Sakurai, M., Komori, T., Fujimoto, T., Ito, G., Yoshimura, S.-ichiro, Harada, A., Fukuda, M., Koike, M., & Iwatsubo, T. (2018). LRRK2 and its substrate RAB GTPases are sequentially targeted onto stressed lysosomes and maintain their homeostasis. *Proceedings of the National Academy of Sciences*, *115*(39). https://doi.org/10.1073/pnas.1812196115

Chapter 3: Endogenous Rab38 regulates LRRK2 localization

The Rab (Ras-associated binding) protein family is the largest family of monomeric GTPases (1). They play an important role in vesicular trafficking, both spatially and temporally, in a number of different cell types. For example, Rab proteins regulate several critical processes in immune cells including the transport of immune receptors and the secretion of chemokines and cytokines (2). Importantly, Rab proteins are expressed in neuronal cells where they are involved in several critical vesicular trafficking events, most notably by regulating neuronal development through axonal elongation, axonal polarization and control of both pre- and post-synaptic function (2, 3). Each of these processes involves cooperation between multiple members of the Rab family, which has over 60 members in eukaryotes (4).

LRRK2-substrate interaction is an important and understudied area in the research of pathogenic LRRK2. Not only because it is important to understand which proteins are phosphorylated by LRRK2, but also because substrates can augment LRRK2 kinase activity as well. Previous literature shows that LRRK2 is able to phosphorylate 14 Rab proteins at a conserved site in the Rab's effector binding switch II domain (5). Rab29 is one of these LRRK2 substrates and notably the Rab29 gene is located within the PARK16 genetic locus, named so for its association to PD risk. Recent research has shown that Rab29 recruits overexpressed LRRK2 to the trans-golgi network where it strongly increases its kinase activity (6). Further, overexpression of Rab29 has been shown to rescue the G2019S-induced neurite outgrowth defect, similarly to TRIM1 (7). It seems likely that Rab29 enhances LRRK2 kinase activity by bringing it to the cell membrane where it is more active. This is evidenced by mitochondria-binding Rab29 still increasing LRRK2 kinase activity, also indicating that this effect is not organelle specific (8). Additionally, it must be noted that knockout of endogenous

Rab29 does not affect endogenous LRRK2 kinase activity in a number of cell types and transgenic overexpression in mouse models does not cause an increase in endogenous LRRK2 kinase activity (9). However, more recent work has shown that Rab29 knockdown in RAW264.7 cells does reduce LRRK2 kinase activity, indicating that this interaction may be cell-type specific (10). Given that Rab29 has an established interaction with LRRK2 in various cell systems, our lab has taken interest in Rab32 and Rab38, homologs of Rab29 that may also regulate LRRK2 localization and kinase activity.

There are a number of links already established between Rab32/Rab38 and LRRK2, such as literature showing that Rab32 and Rab38 interact with LRRK2's Armadillo repeat domain and that Rab32 can be co-immunoprecipitated with LRRK2 in NIH3T3 cells (11, 12). As described in Chapter 1, Rab32 shares 56% identity with Rab29 and Rab38 shares 52% identity with Rab29, although they are not as highly expressed in most cell lines. However, Rab32 and Rab38 do show high expression in cells that produce lysosome-related organelles (LROs) (13, 14). Previous research in alveolar type II pneumocytes, which have high expressions of both Rab38 and LRRK2, has shown that Rab38-deficient mutant rats develop a buildup of surfactant in the lungs due to a dysfunction of Lamellar bodies, a type of LRO. Importantly, the same surfactant phenotype is observed with LRRK2 kinase inhibitor treatment, suggesting both LRRK2 and Rab38 are involved in this LRO biogenesis pathway (15, 16).

Much of my early research involved LRRK2 and Rab interactions, primarily focusing on Rab32 and Rab38 in HEK-293T cells. These experiments didn't produce many valuable results, so we eventually tried other cell lines with higher endogenous expression of Rab32, Rab38 and LRRK2. B16-F10 mouse melanocytes made a great candidate cell line because of their high endogenous expression for Rab32, Rab38 and LRRK2 as well as their production of LROs called

melanosomes. As mentioned, LROs are of great interest because both Rab32 and Rab38 are important for LRO biogenesis and LRRK2 is likely involved here as well (16, 17).

Materials and Methods

Cell culture

All cells were grown at 37°C and 5% CO_2 in a humidified incubator. B16-F10 mouse melanocytes were grown in RPMI-1640 + 10% FBS.

Plasmids and Transfection

We thank Dr. Dario Alessi for providing the following plasmids: pcDNA5 FRT/TO, pcDNA5 FRT/TO mCherry-LRRK2 (DU52361), pcDNA5 FRT/TO GFP-LRRK2 (DU13363), pCMV5D-HA-Rab29 (DU50222), pCMV5D-HA-Rab32 (DU52622), pCMV5D-HA-Rab38 (DU52517, pCMV5D-GFP-Rab29 (DU50223). We also thank Marci Scidmore and William Pavan for donating EGFP-Rab32 and DV-GFP-Rab38-WT-pDEST53 respectively.
All transfections were performed using Lipofectamine 2000 (Invitrogen, 11668019) at a ratio of 2µl of Lipofectamine 2000 per 1µg of plasmid DNA. Cells were plated such that when transfected the following day, they were between 60-80% confluent. Cells were left in transfection media for 6-24 hours.

siRNA Knockdown

siRNA transfection was performed using electroporation with Amaxa Nucleofection or by using Lipofectamine RNAiMAX (Thermo Fisher, 13378075). For electroporation, the Amaxa Nucleofector II machine and Cell Line Nucleofector Kit V (Lonza Bioscience, VCA-1003) were used to transfect 1uM of siRNA. For B16-F10 cells, the P-020 program was used on the Amaxa Nucleofector II. When transfecting the siRNA with Lipofectamine RNAiMAX, siRNA was

introduced at a final concentration of 10nM and 0.3µL of RNAiMAX transfection reagent was used per pmol of siRNA. After 6-24 hours transfection media was replaced with fresh media containing no transfection reagent. After an additional 48-72 hour incubation, the cells were harvested by scraping. Lastly, any residual media was washed with PBS. The siRNAs used were mouse siGENOME SMARTpool siRNAs from Horizon Discovery: scrambled control (D-001206-13-05), LRRK2 (M-049666), Rab29 (M-053101), Rab32 (M-063539) and Rab38 (M-040873).

Cell Lysis

Cells were resuspended in ice-cold lysis buffer comprised of 50 mM Tris, pH 7.5, 150 mM NaCl, 1 mM EDTA, and 0.5% NP-40 supplemented with Phosstop phosphatase inhibitor (Roche, 04906845001) and cOmplete protease inhibitor (Roche, 11836170001). The cells were then incubated on a rotator at 4°C for 30 minutes. After incubation, cells were centrifuged for 5 minutes at 4°C to clear cell debris. The supernatant was separated and its protein concentration was determined with the Pierce BCA Protein Assay Kit (Thermo Fisher Scientific, 23225). The samples' protein concentrations were then normalized.

Immunoblotting

NuPAGE LDS loading buffer with 5% β-mercaptoethanol was added to the normalized lysates and the solution was incubated at 70-95°C for 5-10 mins to denature. The cells were then run on NuPage 4-12% Bis-Tris (Invitrogen, NP0321) and/or 3-8% Tris-acetate (Invitrogen, EA0375) polyacrylamide gels, depending on the molecular weight of the target protein. After running, the gels were transferred onto PVDF membranes (EMD Millipore, IPFL00010) with the Genscript eBlot L1 transfer system. Membranes were blocked with Intercept TBS blocking buffer (LI-COR, 927-60001) for 30 minutes. The primary antibodies used were: mouse

anti-LRRK2 N241 [Antibodies Inc. 75-253], rabbit anti-LRRK2 C41-2 (Abcam, ab133474), rabbit anti-LRRK2 pS1292 (Abcam, ab203181), mouse anti-Rab8A (Santa Cruz, 81909), rabbit anti-Rab8A pT72 (Abcam, 230260), mouse anti-Rab10 (Sigma, SAB5300028), rabbit anti-Rab10 pT73 (Abcam, ab230261), mouse anti-Rab12 (Santa Cruz, 515613), rabbit anti-Rab12 pS106 (Abcam, 256487), rabbit anti-Rab29 (Abcam, ab256526), mouse anti-Rab32 (Santa Cruz, 390178), rabbit anti-Rab38 (Cell Signaling, 14365S), rabbit anti-GFP (Abcam, ab290) and rabbit anti-actin (Cell Signaling, clone 13E5, 4970). All primary antibodies were diluted 1:1000, except for the actin antibody which was diluted at 1:5000. Membranes were incubated in primary for either 3 hours at room temperature or overnight at 4°C. The secondary antibodies, IRDye 800CW goat anti-mouse (LI-COR, 926-32210) and 680RD goat anti-rabbit (LI-COR, 926-68071) were diluted 1:10,000 and incubated for 30 minutes at room temperature. The LI-COR Odyssey CLx system was used to image and quantify fluorescence, which was then interpreted using Image Studio acquisition software.

Immunofluorescence

For immunofluorescence assays, B16-F10 cells were plated on 35mm poly-D-lysine coated coverslip dishes (MatTek, P35GC-0-14-C). Transfection and/or siRNA knockdown was performed on the cells as described. The following day, the cells were first fixed by incubation in a 4% Paraformaldehyde solution in PBS supplemented with 0.2M sucrose for 10 minutes. They were then washed with 0.2% BSA in PBS, which was followed by incubation in a blocking buffer of 5% donkey serum solution (Jackson ImmunoResearch, 017-3000-121). After blocking, the primary antibodies used were: mouse-anti Rab32 (Santa Cruz, 390178), rabbit anti-Rab38 (gift from Santiago Di Pietro), mouse anti-Rab10 (Sigma, SAB5300028), and rabbit anti-Rab10 phospho T73 (Abcam, ab230261). Cells were incubated in primary antibody at room temperature

for 1 hour, all at a dilution of 1:200 except for Rab38 which was diluted 1:1000. All antibodies were diluted in a solution of 1% BSA and 0.3% Triton X-100 in PBS. After primary antibody incubation, the cells were washed with 0.2% BSA in PBS three times followed by incubation in secondary antibody. Secondary antibodies used were: AlexaFluor647 AffiniPure donkey anti-mouse IgG (Jackson ImmunoResearch, 715-605-151), Rhodamine RedX (RRX) AffiniPure donkey anti-mouse IgG (Jackson ImmunoResearch, 715-295-150), AlexaFluor647 AffiniPure donkey anti-rabbit IgG (Jackson ImmunoResearch, 711-605-152), Rhodamine RedX (RRX) AffiniPure donkey anti-rabbit IgG (Jackson ImmunoResearch, 711-295-152). Secondary antibodies were diluted 1:200 in the same solution as primary antibodies. The Olympus IX-80 Fluoview 1000 laser scanning confocal microscope was used to image, with a 60x oil-immersion objective. Images were typically taken at a resolution of 1024x1024 pixels and z-stacks used a step size of 0.5-1um. Images were processed using the Fiji image processing package.

Quantification of Microscopy

50 images were taken per plate for each quantified plate. The criteria for cells to be imaged and used in quantification were: the cells were securely adherent, had a clearly defined nucleus, showed the expected morphology indicative of cell health, showed neither exceptionally high or low fluorescence signal and had limited nonspecific aggregates. The individual taking the images was blinded to conditions. The criteria for quantification of perinuclear LRRK2 or Rab32 aggregation was the presence of a concentrated punctate cluster of fluorescent signal near the nucleus. If there was any uncertainty in the presence of a perinuclear aggregate, cells were counted as not having it. For each replicate, the proportion of cells with perinuclear LRRK2 or Rab32 was calculated. Data was reported as the average across replicates, with error represented by the standard error of the mean.

Results

LRRK2 exhibits pericentriolar localization in B16-F10 mouse melanocytes.

I found that in B16-F10 cells, overexpressed LRRK2 shows a high amount of pericentriolar localization instead of the typical diffuse cytoplasmic localization. Immunofluorescence staining for the golgi and the centrioles revealed that the GFP-LRRK2 punctate cluster was located within the golgi region, but specifically was very closely associated with the much smaller pericentriolar region (Fig. 1a). Almost all cells which met the criteria for imaging showed this pericentriolar localization of GFP-LRRK2 (97% ± 2%, mean ± SEM).

LRRK2 colocalizes with Rab32 and Rab38 in pericentriolar region of B16-F10 cells.

To further understand Rab protein interaction with LRRK2 in this cell line, I performed an immunofluorescence assay staining for endogenous Rab32 and Rab38 in B16-F10 cells transfected with GFP-LRRK2. This showed that Rab32 colocalizes with GFP-LRRK2 in almost all cells (98% ± 2%). Rab38 also colocalized with LRRK2 in the pericentriolar region but this colocalization was not quantified due to difficulty in obtaining sufficient Rab38 antibody.

Rab38 regulates pericentriolar localization of LRRK2 in B16-F10 cells.

It is known that LRRK2 is recruited to the trans-golgi network by Rab29 overexpression in a number of cell lines (6, 7).Therefore we speculated that the understudied Rab29 homologs Rab32 or Rab38 may similarly regulate LRRK2 localization in cell lines where LRRK2, Rab32 and Rab38 are highly expressed endogenously. To investigate this, I performed siRNA knockdowns of Rab29, Rab32 and Rab38 in B16-F10 cells paired with GFP-LRRK2 overexpression and a scrambled control. I then imaged these plates on a fluorescent confocal microscope to evaluate the effect of Rab knockdown on the observed GFP-LRRK2 pericentriolar localization. With scrambled siRNA knockdown, nearly all GFP-LRRK2 was in a pericentriolar

punctate cluster (94% ± 4%). The same phenotype was observed in Rab29 (96% ± 1%) and Rab32 (92% ± 3%) knockdown (Figs. 2a-c). Upon Rab38 knockdown however, only around half of the cells showed the characteristic pericentriolar GFP-LRRK2 localization (49% ± 3%), with the rest localized diffusely in the cytoplasm (Fig. 2a). Rab38 knockdown greatly reduces but does not completely eliminate endogenous Rab38 expression, which may explain why roughly half of cells still have detectable pericentriolar GFP-LRRK2 (Fig. 2b). This data indicates that Rab38 directly or indirectly controls LRRK2 localization in B16-F10 mouse melanocytes.

Kinase-dead mutants, but not PD pathogenic mutants, disrupt LRRK2 pericentriolar localization in B16-F10 cells.

Most pathogenic LRRK2 mutations lead to increased kinase activity. Therefore, I explored the effect of alterations to kinase activity on LRRK2 pericentriolar localization in B16-F10 cells. I found that mutations which abolish LRRK2 kinase activity disrupt the observed localization. The D2017A kinase dead mutant and the T1348N non-GTP binding kinase inactive mutant showed almost no pericentriolar localization (Figs. 3a and 3b), with almost all cells having diffusely cytoplasmic LRRK2 (1% ± 1% of cells had pericentriolar LRRK2 D2017A, 3% ± 1% of cells had pericentriolar LRRK2 T1348N). The disruption in LRRK2 localization with both of these mutations strongly suggests that LRRK2 kinase activity is essential for LRRK2 pericentriolar localization in B16-F10 cells. Naturally, I also imaged the most pathologically relevant LRRK2 mutants in this cell line to characterize their localization. Confocal microscopy of mutants G2019S, R144C, and Y1699C revealed that these kinase hyperactive mutants cause no alteration to the characteristic pericentriolar punctate cluster. As a baseline, 98% ± 3% of cells had pericentriolar wild type GFP-LRRK2. The mutants localization was unchanged: GFP-LRRK2 G2019S had 97% ± 1%, GFP-LRRK2 R1441C had 97% ± 3% and GFP-LRRK2

Y1699C had 97% ± 0% (Fig. 3c). Further, Rab32 colocalizes with all tested LRRK2 pathogenic mutants but does not colocalize with the kinase inactive mutants D2017A and T1348N (Figs. 3b and 3c).

HPS1 and HPS4 knockdown reduces LRRK2 pericentriolar localization.

HPS1 and HPS4 are components of the Rab38 guanine nucleotide exchange factor (GEF) BLOC-3. BLOC-3 catalyzes the conversion of Rab38 GDP to GTP. siRNA knockdown of either HPS1 or HPS4 disrupts BLOC-3 complex formation, inhibiting Rab38 membrane binding and activity (18). We speculated that inhibition of BLOC-3 complex formation may indirectly inhibit LRRK2 pericentriolar localization and further support our hypothesis that Rab38 regulates LRRK2 localization in this cell line. Upon siRNA knockdown of either HPS1 and HPS4, LRRK2 pericentriolar aggregation was reduced; 34% ± 10% of LRRK2 was pericentriolar with HPS1 knockdown and 33% ± 3% with HPS4 knockdown, compared to 91% ± 2% with scrambled siRNA control (Figs. 4a and 4b). Disruption of BLOC-3 formation inhibiting LRRK2 pericentriolar localization further implicates Rab38 in the regulation of LRRK2 localization in B16-F10 cells.

Discussion

With this work, I have shown that the Rab29 homolog Rab38 is a novel endogenous regulator of LRRK2 localization and that in B16-F10 mouse melanocytes, LRRK2 forms a punctate cluster in the pericentriolar region where it colocalizes with both Rab32 and Rab38. Further, I have shown that kinase activity is required for this LRRK2 localization but overactive pathogenic LRRK2 mutants show no alteration to the characteristic localization pattern. I supported my finding that Rab38 regulates LRRK2 localization by showing that disrupting the

formation of BLOC-3 reduces LRRK2 pericentriolar localization as well. Additional work done by others in our lab has shown that endogenous Rab38 also regulates LRRK2 kinase activity and controls LRRK2 membrane association.

Most importantly, these findings are the first report of a Rab protein endogenously regulating LRRK2 subcellular localization and kinase activity in vivo. Although overexpressed Rab29 has been shown to direct overexpressed LRRK2 to the trans-Golgi where it increases its kinase activity as mentioned, studies investigating the effects of Rab29 knockdown have shown that a decrease in Rab29 levels does not inhibit endogenous LRRK2 kinase activity (9). Our lab's results make clear the importance of cell-type-specific investigation of LRRK2 protein interaction as we have only observed this Rab38-LRRK2 interaction in B16-F10 cells and melan-a cells. It is quite possible that a number of other Rab proteins endogenously regulate LRRK2 but that this interaction has not been probed in the correct cell types. Future work should be done investigating LRRK2-Rab protein interactions in other cell types, especially cell types which have relevance to PD. Based on my results, a great candidate Rab protein for potential LRRK2 interactions in other cell lines is Rab32. While Rab32 knockdown does not impact LRRK2's localization in B16-F10 cells, their clear colocalization indicates that some level of interaction between the two proteins may exist, possibly in another LRO producing cell line.

It must be noted that Rab32 and Rab38 accumulation was only observed when LRRK2 was overexpressed. Therefore, these experiments primarily serve to convey the regulation of LRRK2 by endogenous Rab38 rather than to propose a novel physiological system. However, research showing that disruption of either Rab38 or LRRK2 function in murine models causes the same pathological lung phenotype and that pathogenic LRRK2 has been shown to affect the centrioles indicates that the two proteins may interact in a physiologically relevant manner (16,

19, 20, 21). Future research should attempt to define LRRK2-Rab38 interaction in a physiological context to reveal the true implications of Rab38's regulation of LRRK2.

Our findings regarding LRRK2 pericentriolar localization align with a recent study showing that N-terminal lysines of LRRK2 have a high affinity for LRRK2-phosphorylated Rab10 and Rab8 (22). It is important to note that work done by others in our lab has also shown that Rab10 phosphorylated at T73 colocalizes with LRRK2 in the pericentriolar region. Literature has also shown LRRK2-phosphorylated Rab10 to be recruited to the pericentriolar region, which may help explain why we have found high levels of LRRK2, Rab10, Rab32 and Rab38 there as well (23). This could be described by a potential mechanism where active LRRK2 associates with LRRK2-phosphorylated Rab proteins at membranes, and thus more Rab proteins get phosphorylated in this small region causing more LRRK2 association in a feedback loop (22). This mechanism might also explain why we observed that kinase inactive LRRK2 mutants do not localize to the pericentriolar region and do not colocalize with Rab32, because they would not be able to trigger this sort of feedback loop. Given the regulatory relationship that Rab29, Rab38 and possibly other Rab proteins hold over LRRK2, this possibility should be of great interest due to its potential effects on LRRK2 kinase activity and therefore pathogenesis.

Figure 3.1: GFP-LRRK2 colocalizes with endogenous Rab32, Rab38 and phosphorylated Rab10 in the pericentriolar region of B16-F10 cells. (A) Confocal microscopy imaging of an immunofluorescence assay staining for pericentrin (centrioles) and giantin (golgi) in B16-F10 cells shows that GFP-LRRK2 localizes to the pericentriolar region. The final image of each set is an overlay of all 3 channels. (B) Confocal microscopy imaging of an immunofluorescence assay staining for endogenous Rab32 and Rab38, along with GFP-LRRK2 transfection in B16-F10 cells. All rows first show the brightfield for each cell. The top row shows Rab32 (magenta), GFP-LRRK2 (green) and an overlaid image (white). The second row shows Rab32 (magenta) without LRRK2 overexpression. The third row shows Rab38 (magenta), GFP-LRRK2 (green) and an overlaid image (white). The bottom row shows Rab38 (magenta) without LRRK2 overexpression. (C) Confocal microscopy imaging of cells transfected with mCherry-LRRK2 (red) and either GFP-alone, GFP-Rab29, GFP-Rab32 or GFP-Rab38 (green) in live B16-F10 cells. Each set also shows the brightfield (left) and an overlaid image (right). Scale bar = 10μm.

Figure 3.1

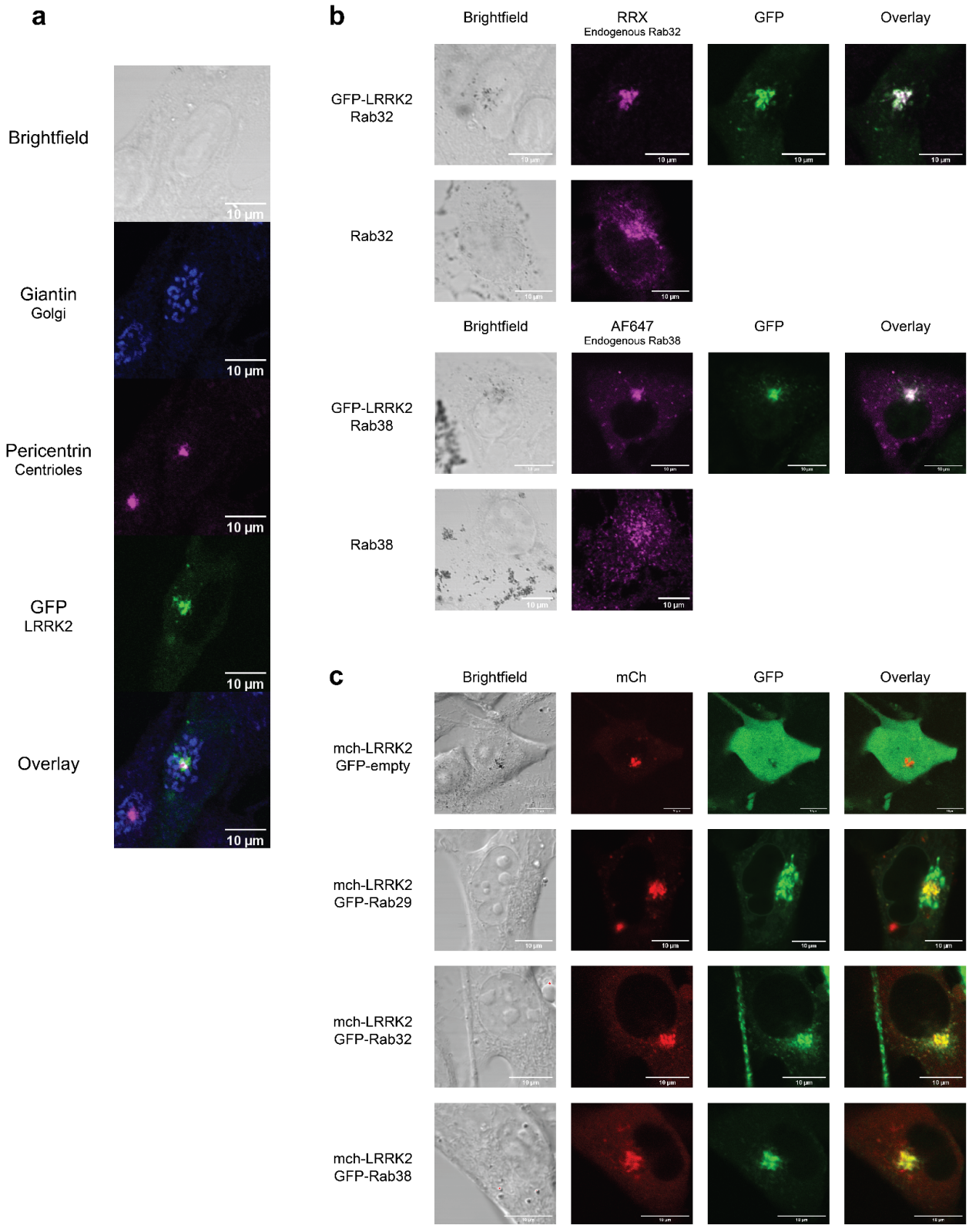
a
Brightfield
Giantin
Golgi
Pericentrin
Centrioles
GFP
LRRK2
Overlay
10 µm
b
Brightfield
RRX
Endogenous Rab32
GFP
Overlay
GFP-LRRK2
Rab32
Rab32
Brightfield
AF647
Endogenous Rab38
GFP
Overlay
GFP-LRRK2
Rab38
Rab38
c
Brightfield
mCh
GFP
Overlay
mch-LRRK2
GFP-empty
mch-LRRK2
GFP-Rab29
mch-LRRK2
GFP-Rab32
mch-LRRK2
GFP-Rab38

Figure 3.2: Rab38 knockdown inhibits LRRK2 pericentriolar localization. (A) Confocal microscopy imaging of B16-F10 cells with an siRNA knockdown of Rab29, Rab32 and Rab38 with overexpressed GFP-LRRK2 and a scrambled control. Scale bar = 10 μm. (B) Quantification of the fraction of cells with pericentriolar LRRK2 (white) and Rab32 (gray) upon siRNA knockdown shown in part (A). Each set consists of 3 replicates with at least 50 cells imaged and quantified per replicate. The scrambled control had 94% ± 4% of cells with pericentriolar LRRK2, Rab29 knockdown had 96% ± 1%, Rab32 knockdown had 92% ± 3% and Rab38 knockdown had 49% ± 3%. The scrambled control had 79% ± 8% of cells with pericentriolar Rab32, Rab29 knockdown had 77% ± 9%, Rab32 knockdown had 32% ± 8% and Rab38 knockdown had 31% ± 11%. The bars show the mean while the error bars show the SEM. (C) Quantification of confirmation of siRNA knockdown for 2 separate experiments. Protein levels for each siRNA knockdown are compared to the scrambled siRNA control sample, which was set to 1 (mean +/- SEM).

Figure 3.2

a

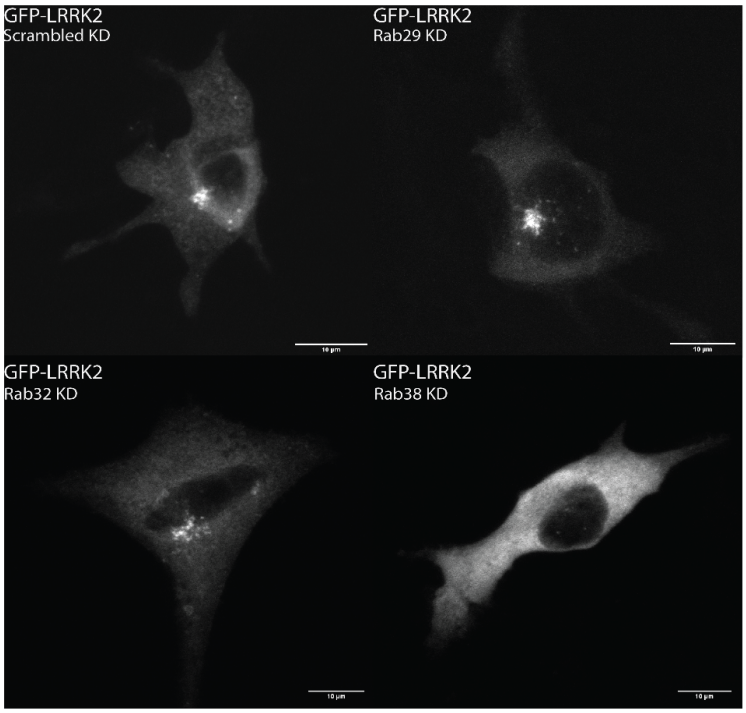

b

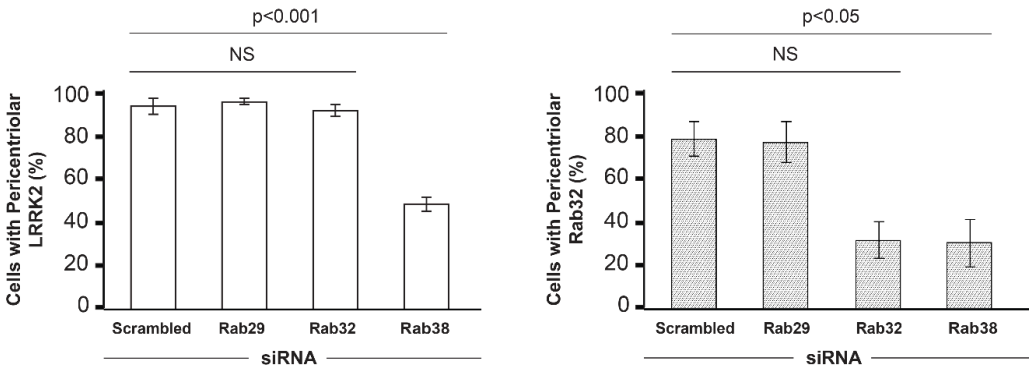

c

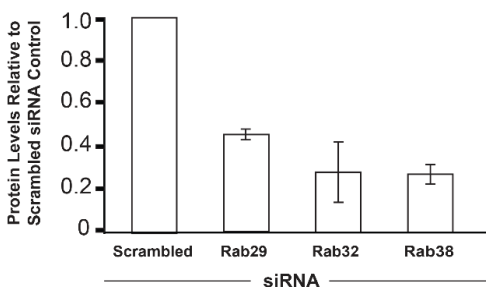

Figure 3.3: Kinase inactive LRRK2 does not localize to the pericentriolar region but overactive mutants show typical pericentriolar localization. (A) Confocal microscopy imaging of an immunofluorescence assay staining for Rab32 (magenta) in B16-F10 cells with overexpressed kinase-inactive LRRK2 mutants D2017A (top) and T1348N (bottom). Both image sets have a brightfield image (left) and an overlaid image (right). Scale bar = 10μm. (B) Quantification of the fraction of cells with pericentriolar LRRK2 (white) and Rab32 (gray) upon transfection with LRRK2-WT, LRRK2-D2017A and LRRK2-T1348N. Each set consists of 3 replicates with at least 50 cells imaged and quantified per replicate. Wild type GFP-LRRK2 had 97% ± 2% of cells with pericentriolar LRRK2, while GFP-LRRK2 D2017A had only 1% ± 1% and GFP-LRRK2 T1348N had only 3% ± 1%. Wild type GFP-LRRK2 had 98% ± 2% with pericentriolar Rab32, while GFP-LRRK2 D2017A had only 0% ± 0% and GFP-LRRK2 T1348N had only 1% ± 1% (mean +/- SEM). (C) Quantification of the fraction of cells with pericentriolar LRRK2 (white) and Rab32 (gray) upon transfection with LRRK2-WT, LRRK2-G2019S, LRRK2-R1441C and LRRK2-Y1699C. Overactive LRRK2 mutants did not affect LRRK2 or Rab32 pericentriolar localization. Wild type GFP-LRRK2 had 98% ± 3% of cells with pericentriolar LRRK2, GFP-LRRK2 G2019S had 97% ± 1%, GFP-LRRK2 R1441C had 97% ± 3% and GFP-LRRK2 Y1699C had 97% ± 0% (mean +/- SEM).

Figure 3.3

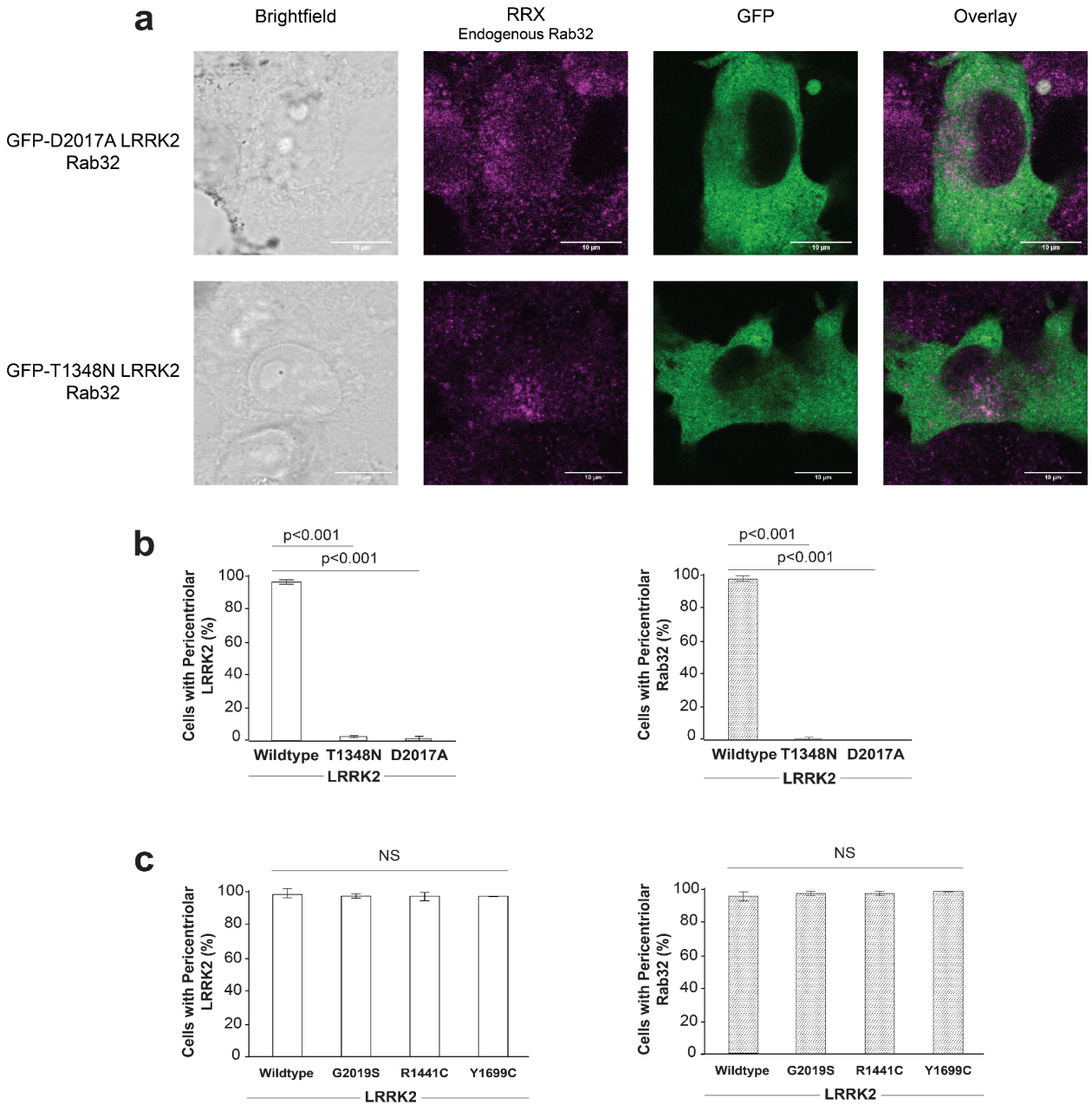
a
Brightfield
RRX
Endogenous Rab32
GFP
Overlay
GFP-D2017A LRRK2
Rab32
GFP-T1348N LRRK2
Rab32
b
p<0.001
p<0.001
Cells with Pericentriolar LRRK2 (%)
Wildtype T1348N D2017A
LRRK2
Cells with Pericentriolar Rab32 (%)
c
NS
Wildtype G2019S R1441C Y1699C

Figure 3.4: Disruption of Rab38 GEF BLOC-3 formation inhibits LRRK2 pericentriolar localization. (A) Confocal microscopy imaging of siRNA knockdown with scrambled (top), HPS1 (middle) and HPS4 (bottom) siRNA in B16-F10 cells transfected with GFP-LRRK2 (green). Scale bar = 10μm. (B) Quantification of the fraction of cells with pericentriolar LRRK2 upon siRNA knockdown shown in part (A). Each set consists of 3 replicates with at least 50 cells imaged and quantified per replicate. With the scrambled siRNA control 91% ± 2% of cells had pericentriolar LRRK2, with HPS1 knockdown 34% ± 10% and with HPS4 knockdown 33% +/- 3% (mean +/- SEM). (C) Quantification of mRNA levels to confirm siRNA knockdown across 3 separate experiments. mRNA levels for each siRNA knockdown are compared to the scrambled siRNA control samples, which were set to 1 (mean +/- SEM).

Figure 3.4

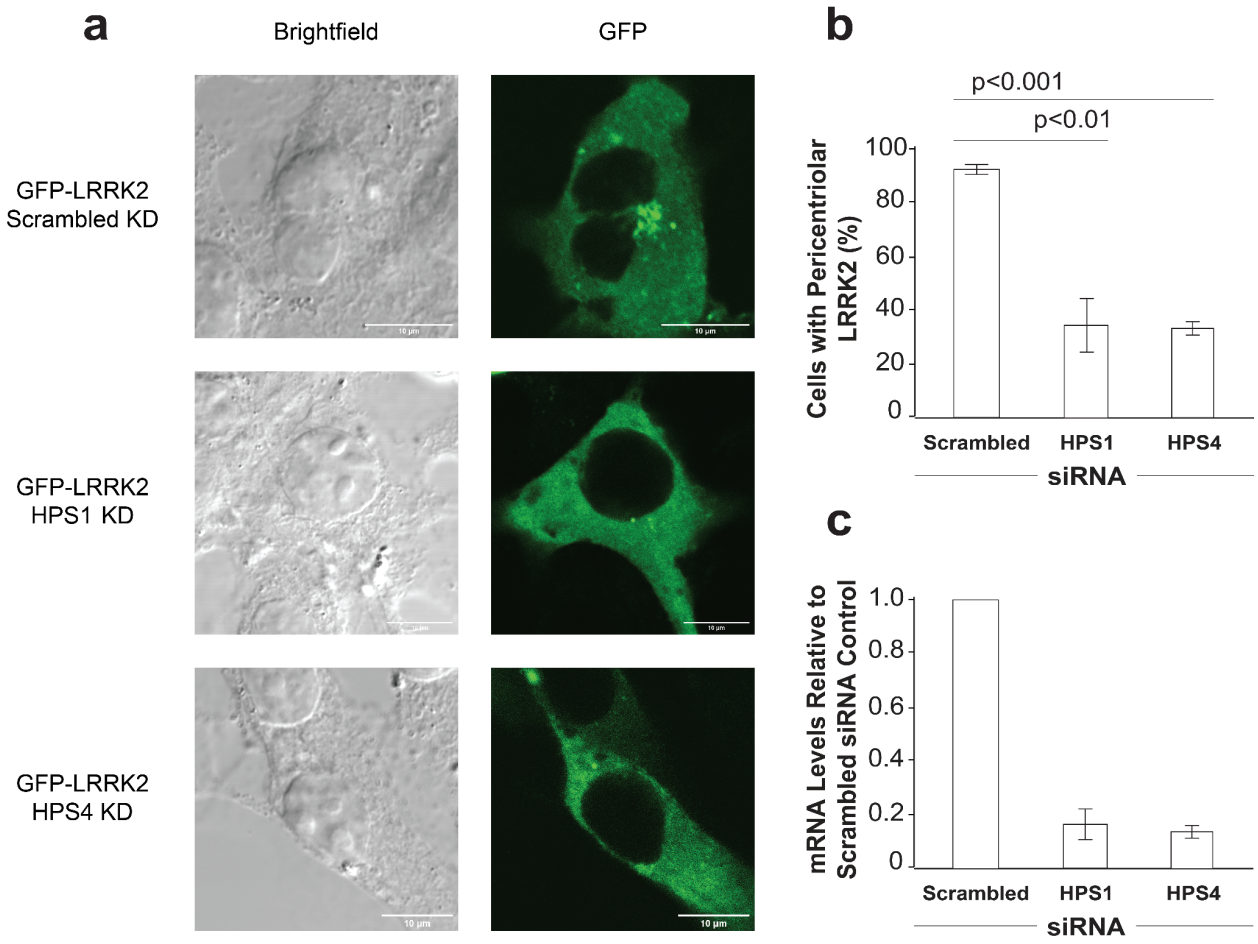
a
Brightfield
GFP
GFP-LRRK2
Scrambled KD
GFP-LRRK2
HPS1 KD
GFP-LRRK2
HPS4 KD
10 µm
b
p<0.001
p<0.01
Cells with Pericentriolar
LRRK2 (%)
100
80
60
40
20
0
Scrambled
HPS1
HPS4
siRNA
c
mRNA Levels Relative to
Scrambled siRNA Control
1.0
0.8
0.6
0.4
0.2
0
Scrambled
HPS1
HPS4
siRNA

References

1. Zerial, M., & McBride, H. (2001). Rab proteins as membrane organizers. *Nature Reviews Molecular Cell Biology*, *2*(2), 107–117. https://doi.org/10.1038/35052055

2. Guadagno, N. A., & Progida, C. (2019). Rab GTPases: Switching to Human Diseases. *Cells*, *8*(8), 909. https://doi.org/10.3390/cells8080909

3. Mignogna, M. L., & D'Adamo, P. (2018). Critical importance of RAB proteins for synaptic function. *Small GTPases*, *9*(1-2), 145–157. https://doi.org/10.1080/21541248.2016.1277001

4. Stenmark, H., & Olkkonen, V. M. (2001). The Rab GTPase family. *Genome biology*, *2*(5), REVIEWS3007. https://doi.org/10.1186/gb-2001-2-5-reviews3007

5. Steger, M., Diez, F., Dhekne, H. S., Lis, P., Nirujogi, R. S., Karayel, O., Tonelli, F., Martinez, T. N., Lorentzen, E., Pfeffer, S. R., Alessi, D. R., & Mann, M. (2017). Systematic proteomic analysis of LRRK2-mediated Rab GTPase phosphorylation establishes a connection to Ciliogenesis. *ELife*, *6*. https://doi.org/10.7554/elife.31012

6. Purlyte, E., Dhekne, H. S., Sarhan, A. R., Gomez, R., Lis, P., Wightman, M., Martinez, T. N., Tonelli, F., Pfeffer, S. R., & Alessi, D. R. (2018). Rab29 activation of the Parkinson's disease-associated LRRK2 kinase. *The EMBO journal*, *37*(1), 1–18. https://doi.org/10.15252/embj.201798099

7. MacLeod, D. A., Rhinn, H., Kuwahara, T., Zolin, A., Di Paolo, G., McCabe, B. D., Marder, K. S., Honig, L. S., Clark, L. N., Small, S. A., & Abeliovich, A. (2013). RAB7L1 interacts with LRRK2 to modify intraneuronal protein sorting and Parkinson's disease risk. *Neuron*, *77*(3), 425–439. https://doi.org/10.1016/j.neuron.2012.11.033

8. Gomez, R. C., Wawro, P., Lis, P., Alessi, D. R., & Pfeffer, S. R. (2019). Membrane association but not identity is required for LRRK2 activation and phosphorylation of Rab GTPases. *The Journal of cell biology*, *218*(12), 4157–4170. https://doi.org/10.1083/jcb.201902184

9. Kalogeropulou, A. F., Freemantle, J. B., Lis, P., Vides, E. G., Polinski, N. K., & Alessi, D. R. (2020). Endogenous Rab29 does not impact basal or stimulated LRRK2 pathway activity. *The Biochemical journal*, *477*(22), 4397–4423. https://doi.org/10.1042/BCJ20200458

10. Eguchi, T., Kuwahara, T., Sakurai, M., Komori, T., Fujimoto, T., Ito, G., Yoshimura, S. I., Harada, A., Fukuda, M., Koike, M., & Iwatsubo, T. (2018). LRRK2 and its substrate Rab GTPases are sequentially targeted onto stressed lysosomes and maintain their homeostasis. *Proceedings of the National Academy of Sciences of the United States of America*, *115*(39), E9115–E9124. https://doi.org/10.1073/pnas.1812196115

11. McGrath, E., Waschbüsch, D., Baker, B. M., & Khan, A. R. (2021). LRRK2 binds to the Rab32 subfamily in a GTP-dependent manner *via* its armadillo domain. *Small GTPases*, *12*(2), 133–146. https://doi.org/10.1080/21541248.2019.1666623

12. Waschbüsch, D., Michels, H., Strassheim, S., Ossendorf, E., Kessler, D., Gloeckner, C. J., & Barnekow, A. (2014). LRRK2 transport is regulated by its novel interacting partner Rab32. *PloS one*, *9*(10), e111632. https://doi.org/10.1371/journal.pone.0111632

13. Wasmeier, C., Romao, M., Plowright, L., Bennett, D. C., Raposo, G., & Seabra, M. C. (2006). Rab38 and Rab32 control post-Golgi trafficking of melanogenic enzymes. *The Journal of cell biology*, *175*(2), 271–281. https://doi.org/10.1083/jcb.200606050

14. Loftus, S. K., Larson, D. M., Baxter, L. L., Antonellis, A., Chen, Y., Wu, X., Jiang, Y., Bittner, M., Hammer, J. A., & Pavan, W. J. (2002). Mutation of melanosome protein RAB38 in chocolate mice. *Proceedings of the National Academy of Sciences*, *99*(7), 4471–4476. https://doi.org/10.1073/pnas.072087599

15. Osanai, K., Higuchi, J., Oikawa, R., Kobayashi, M., Tsuchihara, K., Iguchi, M., Huang, J., Voelker, D. R., & Toga, H. (2010). Altered lung surfactant system in a rab38-deficient rat model of Hermansky-Pudlak syndrome. *American Journal of Physiology-Lung Cellular and Molecular Physiology*, *298*(2). https://doi.org/10.1152/ajplung.00242.2009

16. Fuji, R. N., Flagella, M., Baca, M., S. Baptista, M. A., Brodbeck, J., Chan, B. K., Fiske, B. K., Honigberg, L., Jubb, A. M., Katavolos, P., Lee, D. W., Lewin-Koh, S.-C., Lin, T., Liu, X., Liu, S., Lyssikatos, J. P., O'Mahony, J., Reichelt, M., Roose-Girma, M., Sheng, Z., Sherer, T., Smith, A., Solon, M., Sweeney, Z. K., Tarrant, J., Urkowitz, A., Warming, S., Yaylaoglu, M., Shuo, Z., Zhu, H., Estrada, A. A., Watts, R. J. (2015). Effect of selective LRRK2 kinase inhibition on nonhuman primate lung. *Science Translational Medicine*, *7*(273). https://doi.org/10.1126/scitranslmed.aaa3634

17. Bowman, S. L., Bi-Karchin, J., Le, L., & Marks, M. S. (2019). The road to lysosome-related organelles: Insights from Hermansky-Pudlak syndrome and other rare diseases. *Traffic (Copenhagen, Denmark)*, *20*(6), 404–435. https://doi.org/10.1111/tra.12646

18. Gerondopoulos, A., Langemeyer, L., Liang, J. R., Linford, A., & Barr, F. A. (2012). BLOC-3 mutated in Hermansky-Pudlak syndrome is a Rab32/38 guanine nucleotide exchange factor. *Current biology : CB*, *22*(22), 2135–2139. https://doi.org/10.1016/j.cub.2012.09.020

19. Osanai K. (2018). *Rab38* Mutation and the Lung Phenotype. *International journal of molecular sciences*, *19*(8), 2203. https://doi.org/10.3390/ijms19082203

20. Lara Ordónez, A. J., Fernández, B., Fdez, E., Romo-Lozano, M., Madero-Pérez, J., Lobbestael, E., Baekelandt, V., Aiastui, A., López de Munaín, A., Melrose, H. L., Civiero, L., & Hilfiker, S. (2019). RAB8, RAB10 and RILPL1 contribute to both LRRK2

kinase-mediated centrosomal cohesion and ciliogenesis deficits. *Human molecular genetics*, *28*(21), 3552–3568. https://doi.org/10.1093/hmg/ddz201

21. Madero-Pérez, J., Fdez, E., Fernández, B., Lara Ordóñez, A. J., Blanca Ramírez, M., Gómez-Suaga, P., Waschbüsch, D., Lobbestael, E., Baekelandt, V., Nairn, A. C., Ruiz-Martínez, J., Aiastui, A., López de Munain, A., Lis, P., Comptdaer, T., Taymans, J. M., Chartier-Harlin, M. C., Beilina, A., Gonnelli, A., Cookson, M. R., Greggio, E., Hilfiker, S. (2018). Parkinson disease-associated mutations in LRRK2 cause centrosomal defects via Rab8a phosphorylation. *Molecular neurodegeneration*, *13*(1), 3. https://doi.org/10.1186/s13024-018-0235-y

22. Vides, E. G., Adhikari, A., Chiang, C. Y., Lis, P., Purlyte, E., Limouse, C., Shumate, J. L., Spínola-Lasso, E., Dhekne, H. S., Alessi, D. R., & Pfeffer, S. R. (2022). A feed-forward pathway drives LRRK2 kinase membrane recruitment and activation. https://doi.org/10.1101/2022.04.25.489459

23. Xu, L., Nagai, Y., Kajihara, Y., Ito, G., & Tomita, T. (2021). The Regulation of Rab GTPases by Phosphorylation. *Biomolecules*, *11*(9), 1340. https://doi.org/10.3390/biom11091340

Chapter 4: LRRK2 localization and Rab interactions in IFN-γ and chloroquine treated macrophages

After uncovering the relationship between Rab38 and LRRK2 in B16s, our lab decided to continue this area of study with a focus on lysosome related organelles (LRO). It is known that LRRK2 is involved in the lysosomal system, regulating lysosomal maturation and pH for example (1). However, the mechanisms behind LRRK2's role at lysosomes are still poorly understood. As mentioned in previous chapters, research shows that the buildup of surfactant resulting from impaired LRO function in alveolar type II (AT2) cells occurs upon both Rab38 loss of function and LRRK2 kinase inhibition (2, 3). This suggests a relationship between the two proteins that relates to LRO biogenesis, which may also reveal more about LRRK2's role at lysosomes.

In order to study the LRRK2-Rab substrate endolysosomal pathway, I began working with macrophage cell lines because they have relatively high LRRK2 expression, LRRK2 is involved in a number of immune processes, and macrophages react strongly to drug-induced lysosomal stress (4). A recent paper by Eguchi et al. has shown that after treating these cells with the lysosomotropic drug chloroquine, LRRK2 is strongly recruited to the overload-stressed lysosomes where it serves to temper lysosomal enlargement (5). In RAW264.7 cells, lysosomal overload stress causes Rab29 facilitated recruitment of LRRK2 to the lysosome where LRRK2 shows increased kinase activity as well as colocalization with its substrates Rab8 and Rab10 (5). The authors also show that strong recruitment of LRRK2 to the lysosomes following chloroquine treatment allows for visualization of endogenous LRRK2 by immunofluorescence when macrophages are activated with interferon gamma (IFN-γ) (5, 6). IFN-γ is a cytokine that results in increased expression of endogenous LRRK2, among other proteins (7). As mentioned in

previous chapters, a common shortcoming of LRRK2 research is the reliance on overexpression to obtain adequate LRRK2 levels for a number of experimental techniques such as immunofluorescence. Treatment of macrophages with IFN-γ, similarly to treatment with chloroquine, provides us with a new system to study endogenous LRRK2.

Starting out, we attempted to emulate the microscopy imaging results of the Eguchi paper by treating RAW 264.7 cells with IFN-γ and chloroquine (5). I worked to troubleshoot the drug treatment and we were eventually able to replicate the microscopy images. After successfully replicating the drug effect, we tested other cell lines and found that the J774A.1 murine macrophage line had visible LRRK2 at lysosomes with just chloroquine treatment. J774A.1 cells are derived from the ascites of a mouse with reticulum cell sarcoma and are a commonly used cell line in immunology research. After finding we were able to image endogenous LRRK2 in this context, J774A.1 cells became our lab's model system to investigate the effects of siRNA knockdown and chloroquine treatment on LRRK2 function in macrophages.

Materials and Methods

Cell culture

All cells were grown at 37°C and 5% CO_2 in a humidified incubator. RAW 264.7 cells were grown in DMEM, high glucose (Gibco, 11965-092) supplemented with 10% FBS and 1x Glutamax (Gibco, 35050-061). J774A.1 cells were grown in DMEM, high glucose supplemented with 10% FBS.

Drug Treatment

Cells were treated with media containing 10ng/ml of IFN-γ (Cell Signaling, 39127S) 24 hours after plating and were left in IFN-γ media for 48 hours. We have found IFN-γ to be a very

sensitive reagent, thus special care was taken to dilute the IFN-γ and apply to the plates immediately after the aliquot had been thawed. Cells were treated with media containing chloroquine (CQ) (Sigma-Aldrich, C6628-25G) at a concentration of 100uM. Cells were treated roughly 48 hours after IFN-γ stimulation and were left in CQ media for 3 hours. After the 3 hour treatment, the cells were immediately harvested by scraping or fixed for immunofluorescence.

siRNA Knockdown

siRNA transfection was performed with Lipofectamine RNAiMAX (Thermo Fisher, 13378075). siRNA was introduced to obtain a final concentration of 10nM, and 0.3μL of RNAiMAX transfection reagent was used per pmol of siRNA. After 6-24 hours transfection media was replaced with fresh media containing no transfection reagent or containing drug treatments described above. After an additional 48-72 hour incubation, the cells were harvested by scraping or fixed with PFA fixative for immunofluorescence. The siRNAs used were mouse siGENOME SMARTpool siRNAs from Horizon Discovery: scrambled control (D-001206-13-05), LRRK2 (M-049666), Rab29 (M-053101), Rab32 (M-063539).

Cell Lysis and Immunoblotting

Refer to Chapter 3 Materials and Methods.

Immunofluorescence

Refer to Chapter 3 Materials and Methods. Additionally, in this chapter I used the LAMP1 (BioRad, CD107a) antibody for visualizing lamellar bodies.

Results

LRRK2 is recruited onto enlarged lysosomes upon chloroquine treatment in RAW 264.7 and J774A.1 cells.

I was able to replicate the recruitment of LRRK2 onto enlarged lysosomes in RAW264.7 cells treated with IFN-γ and chloroquine, as described in (5) (Fig. 1a). When implementing this immunofluorescence protocol on chloroquine treated J774A.1 macrophages, I saw that the lysosome-localized LRRK2 phenotype could be visualized without the need for IFN-γ stimulation. Upon chloroquine treatment alone, endogenous LRRK2 is recruited onto enlarged lysosomes in J774A.1 cells (Fig. 1b). These experiments identified J774A.1s as a useful macrophage line to study the effects of lysosomotropic drug treatment on LRRK2 localization and activity.

LRRK2 substrate phosphorylation is stimulated by IFN-γ treatment and is inhibited by both Rab29 and Rab32 knockdown in RAW 264.7 cells.

siRNA knockdown of Rab29 by Eguchi et al. 2018 has shown that Rab29 controls recruitment of LRRK2 onto stressed lysosomes in RAW264.7 cells (5). While this effect was not observed by these researchers following Rab32 knockdown in this cell line, our lab remained curious about a potential role for Rab32 in macrophages. We treated RAW 264.7 cells with IFN-γ and performed an siRNA knockdown of relevant Rab proteins. This first revealed that LRRK2 kinase activity, as measured by Rab10 phosphorylation, was stimulated more than 2 fold by IFN-γ treatment as expected (Figs. 2a and 2c). More importantly, this showed that both Rab29 and Rab32 knockdown inhibited LRRK2 kinase activity in IFN-γ treated samples (Figs. 2a and 2c). Notably, we did not investigate the effects of Rab38 knockdown as it is not expressed in

macrophage cells. Nevertheless, these findings suggest a potential Rab32-LRRK2 interaction pathway in RAW 264.7 cells.

LRRK2 substrate phosphorylation is greatly stimulated by chloroquine and IFN-γ treatment, but is not affected by either Rab29 or Rab32 knockdown in J774A.1 cells.

I continued the investigation into the effects of drug treatment and Rab siRNA knockdown in the J774A.1 cell line. I found that chloroquine treatment resulted in a striking increase in phosphorylated Rab10 signal, with roughly a 10 fold increase on average across all siRNA treatments, with a good deal of variance (Fig. 3c). However, unlike the RAW 264.7 macrophage line, neither Rab29 nor Rab32 knockdown in J774A.1 macrophages caused a decrease in Rab10 phosphorylation (Figs. 3a and 3c). A fellow lab member performed a similar experiment with IFN-γ treatment, which yielded the same result (Fig. 3d). This indicates that Rab-LRRK2 interactions are very cell-type specific, even showing differences between macrophage lines.

Discussion

This work builds on prior research to show that the chloroquine-induced recruitment of LRRK2 onto enlarged lysosomes occurs in other macrophage lines, particularly J774A.1 cells. This is important because J774A.1 cells' high endogenous LRRK2 expression allows for visualization of non-IFN-γ treated endogenous LRRK2 by immunofluorescence, making it a valuable system for LRRK2 research. I have also shown that Rab29 and Rab32 knockdown in IFN-γ-stimulated RAW 264.7 macrophages inhibits LRRK2 kinase activity as measured by Rab10 phosphorylation. Yet surprisingly, Rab29 and Rab32 regulation of LRRK2 kinase activity was not observed in J774A.1 macrophages following either IFN-γ or chloroquine treatment.

Current literature regarding Rab29 regulation of LRRK2 function in the chloroquine induced lysosomal stress system remains divided. It is apparent that chloroquine treatment results in LRRK2 translocation to the lysosomes and a sharp increase in LRRK2 kinase activity, measured by phosphorylation of Rab10 and Rab12. Work done by Eguchi et al. 2018 shows that Rab29 is critical for LRRK2 recruitment to the lysosomes in this system in RAW 264.7 cells (5). However, Alessi et al. 2020 has shown that siRNA knockdown of Rab29 in chloroquine-treated mouse embryonic fibroblasts has no effect on LRRK2 kinase activity (8). Here, I have shown that Rab29 knockdown inhibits LRRK2 kinase activity in IFN-γ treated RAW 264.7 cells. However, our knockdowns in J774A.1s indicate that neither Rab29 nor Rab32 regulate LRRK2 kinase activity in this line following either chloroquine or IFN-γ treatment. In accordance with previous chapters, these results suggest that Rab regulation of LRRK2 is very cell-type-specific. Future studies could expand similar investigations of LRRK2 activity into other macrophage lines and possibly uncover details of LRRK2's role in macrophages.

In the paper which inspired this work, the findings about LRRK2 are in the light of IFN-γ treatment, as are my findings regarding the regulation of LRRK2 kinase activity by Rab29 and Rab32 in RAW 264.7 cells. This is important to note because IFN-γ is the primary activator of macrophages and thus has several effects beyond stimulating LRRK2 expression (9, 10, 11). For example, upon microscopy imaging of IFN-γ treated RAW 264.7s the cells typically show clear morphological changes, appearing much larger with exaggerated and more numerous projections. There is also evidence indicating that IFN-γ treatment in macrophages may result in abnormal LRRK2 cleavage which can affect LRRK2 localization and kinase activity (12). Our lab's investigations into LRRK2 cleavage in this system have shown it to be inconsistent but

future studies should be done to detail this understudied aspect of LRRK2 biology in macrophages.

While the effect of Rab29 and Rab32 knockdown on LRRK2 kinase activity in the J774A.1 line was not statistically significant, there did seem to be an increase in Rab10 phosphorylation following Rab32 knockdown. This made me curious about a possible relationship between Rab32 and LRRK2 in this line as well. Upon further statistical analysis, I found that a near-significant and consistent increase in LRRK2 levels was observed following Rab32 knockdown. Given that my results are derived from a limited number of experiments, I believe that further study into this point could reveal a novel endogenous relationship between Rab32 and LRRK2 in macrophages.

It was expressed earlier that our interest in lamellar bodies comes from studies suggesting a potential shared pathway between LRRK2 and Rab38 in AT2 cells involving lamellar bodies, and it is known that Rab38 is important for lamellar body maturation (13). However, studying AT2 cells can be challenging because cultured AT2 cells typically have reduced ability to produce lamellar bodies and surfactant. However, a recent study improved lamellar body size in cultured AT2 cells by exogenous expression of mCherry-ABCA, a lamellar body protein (14). I attempted to integrate a GFP-ABCA construct with several different selections into mouse lung epithelial (MLE-15) cells for several months but was unable to develop a stably integrated line. Typically, the cells would express GFP-ABCA in structures resembling lamellar bodies but would lose their GFP signal after a few days. Eventually, I abandoned this project to focus on other aspects of LRRK2's relationship to the lysosome and LROs. Nevertheless, there still exists an opportunity for future studies to explore LRRK2 and Rab38's relationship with lamellar bodies.

Figure 4.1: Chloroquine treatment causes LRRK2 recruitment onto enlarged lysosomes in RAW 264.7 and J774A.1 macrophages. (A) Confocal microscopy imaging of an immunofluorescence assay revealing endogenous LRRK2 with the C41-2 antibody and lamellar bodies with an antibody for LAMP1. Left to right shows brightfield, C41-2 (green), LAMP1 (red) and an overlaid image of C41-2 and LAMP1. Top to bottom shows RAW 264.7 cells which are untreated, treated with IFN-γ, treated with chloroquine and treated with both IFN-γ and chloroquine. (B) The same as (A) but with J774A.1 cells. Scale bars = 10um.

Figure 4.1

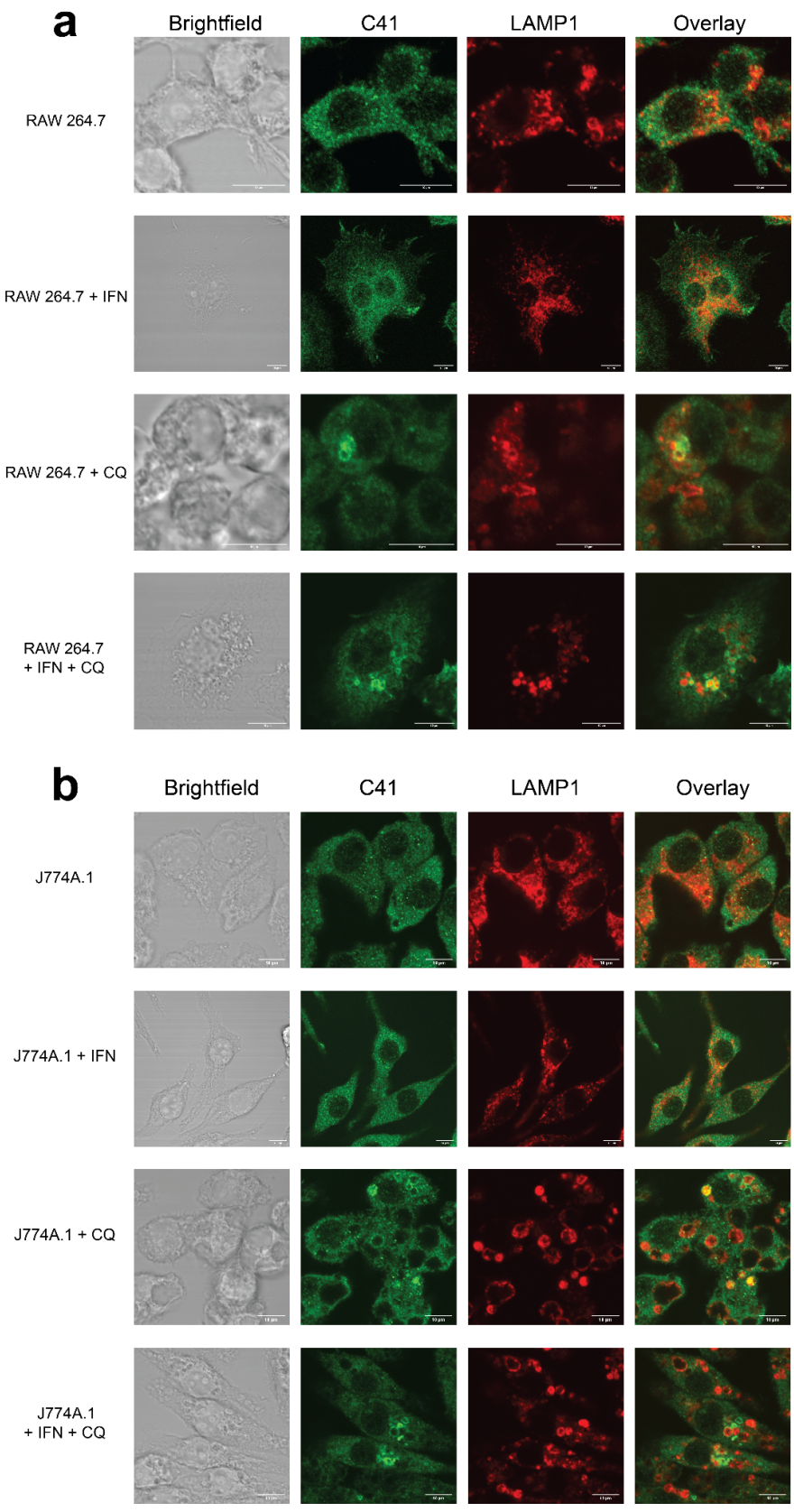
a
Brightfield
C41
LAMP1
Overlay
RAW 264.7
RAW 264.7 + IFN
RAW 264.7 + CQ
RAW 264.7
+ IFN + CQ
b
Brightfield
C41
LAMP1
Overlay
J774A.1
J774A.1 + IFN
J774A.1 + CQ
J774A.1
+ IFN + CQ

Figure 4.2: Rab29 and Rab32 knockdown inhibit LRRK2 kinase activity in IFN-γ treated RAW 264.7 cells. (A) LRRK2 kinase activity as measured by phosphorylated Rab10 over total Rab10 for each siRNA knockdown and drug treatment, all relative to the untreated scrambled siRNA control. phospho-T73/Rab10 in untreated cells relative to the untreated scrambled control was 80.4% ± 1.8% following Rab29 knockdown and 87.4% ± 3.6% following Rab32 knockdown. phospho-T73/Rab10 in IFN-γ treated scrambled siRNA samples was 251.0% ± 9.6% compared to the untreated control. phospho-T73/Rab10 in IFN-γ treated cells relative to the untreated scrambled control was 84.7% ± 1.2% following Rab29 knockdown and 121.8% ± 0.4% following Rab32 knockdown. (B) Protein levels relative to untreated and IFN-γ treated scrambled control. Rab29 knockdown in untreated cells reduced Rab29 levels to 44.5% ± 3.7% and Rab32 knockdown in untreated cells reduced Rab32 levels to 16.8% ± 1.7% relative to the untreated scrambled control. Rab29 knockdown in IFN-γ treated cells reduced Rab29 levels to 34.7% ± 2.7% and Rab32 knockdown in IFN-γ treated cells reduced Rab32 levels to 11.1% ± 2.4% relative to the IFN-γ treated scrambled control. (C) A representative immunoblot which data in this figure was drawn from.

Figure 4.2

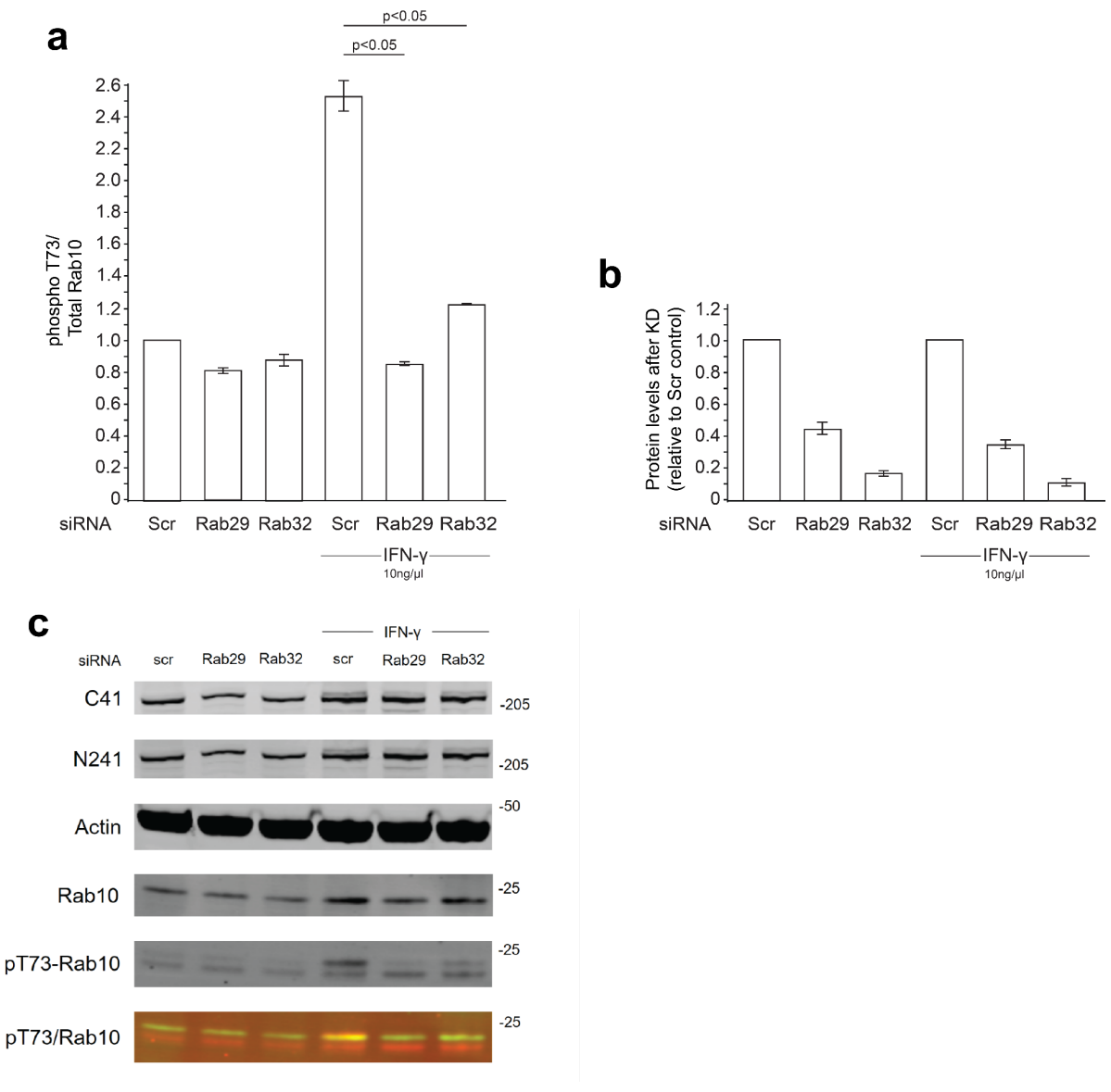
a
p<0.05
p<0.05
phospho T73/
Total Rab10
2.6
2.4
2.2
2.0
1.8
1.6
1.4
1.2
1.0
0.8
0.6
0.4
0.2
0
siRNA
Scr
Rab29
Rab32
Scr
Rab29
Rab32
IFN-γ
10ng/μl
b
Protein levels after KD
(relative to Scr control)
1.2
1.0
0.8
0.6
0.4
0.2
0
siRNA
Scr
Rab29
Rab32
Scr
Rab29
Rab32
IFN-γ
10ng/μl
c
IFN-γ
siRNA
scr
Rab29
Rab32
scr
Rab29
Rab32
C41
-205
N241
-205
Actin
-50
Rab10
-25
pT73-Rab10
-25
pT73/Rab10
-25

Figure 4.3: Rab29 and Rab32 knockdown does not affect LRRK2 kinase activity in J774A.1 cells, regardless of chloroquine treatment. (A) LRRK2 kinase activity as measured by phosphorylated Rab10 over total Rab10 for each siRNA knockdown and drug treatment, relative to the untreated or chloroquine treated scrambled siRNA control. phospho-T73/Rab10 in untreated cells relative to control was 58.8% ± 2.2% following LRRK2 knockdown, 102.7% ± 10.6% following Rab29 knockdown and 156.6% ± 33.0% following Rab32 knockdown. phospho-T73/Rab10 in chloroquine treated cells relative to chloroquine treated control was 71.4% ± 13.8% following LRRK2 knockdown, 111.2% ± 21.7% following Rab29 knockdown and 124.4% ± 8.4% following Rab32 knockdown. (B) Protein levels relative to untreated and IFN-γ treated scrambled control. In untreated cells, knockdown reduced LRRK2 levels to 41.5% ± 12.2%, Rab29 levels to 44.9% ± 14.0% and Rab32 levels to 36.9% ± 11.8% relative to the scrambled control. In chloroquine treated cells, knockdown reduced LRRK2 levels to 59.6% ± 17.3%, Rab29 levels to 45.1% ± 9.3% and Rab32 levels to 35.4% ± 8.4% relative to the chloroquine treated scrambled control. (C) A representative immunoblot which data in this figure was drawn from. (D) An immunoblot showing that Rab29 and Rab32 knockdown in IFN-γ treated J774A.1 cells similarly does not reduce LRRK2 kinase activity.

Figure 4.3

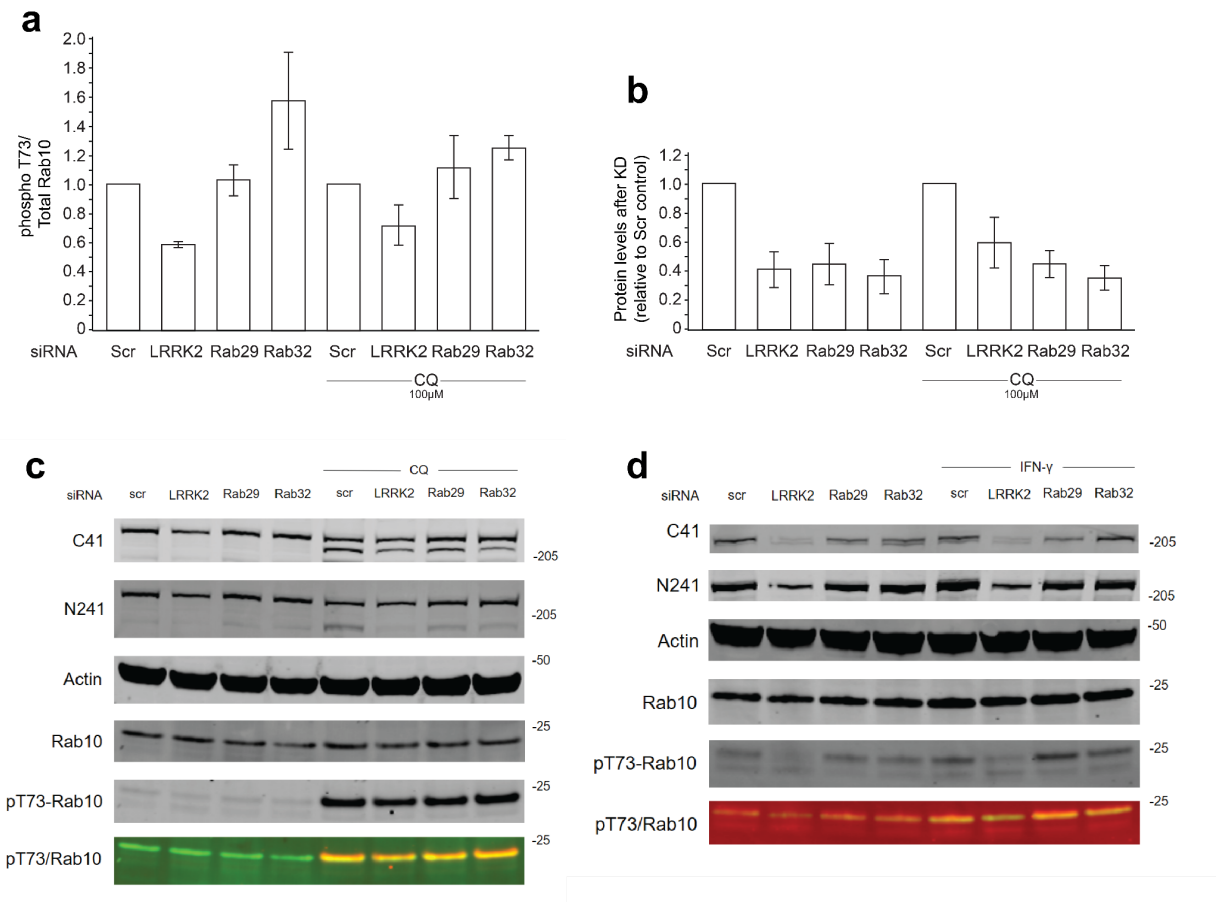
a
phospho T73/
Total Rab10
2.0
1.8
1.6
1.4
1.2
1.0
0.8
0.6
0.4
0.2
0
siRNA
Scr
LRRK2
Rab29
Rab32
Scr
LRRK2
Rab29
Rab32
CQ
100μM
b
Protein levels after KD
(relative to Scr control)
1.2
1.0
0.8
0.6
0.4
0.2
0
siRNA
Scr
LRRK2
Rab29
Rab32
Scr
LRRK2
Rab29
Rab32
CQ
100μM
c
CQ
siRNA
scr
LRRK2
Rab29
Rab32
scr
LRRK2
Rab29
Rab32
C41
N241
Actin
Rab10
pT73-Rab10
pT73/Rab10
-205
-205
-50
-25
-25
-25
d
IFN-γ
siRNA
scr
LRRK2
Rab29
Rab32
scr
LRRK2
Rab29
Rab32
C41
N241
Actin
Rab10
pT73-Rab10
pT73/Rab10
-205
-205
-50
-25
-25
-25

References

1. Madureira, M., Connor-Robson, N., & Wade-Martins, R. (2020). LRRK2: Autophagy and lysosomal activity. *Frontiers in Neuroscience*, *14*. https://doi.org/10.3389/fnins.2020.00498

2. Osanai, K., Higuchi, J., Oikawa, R., Kobayashi, M., Tsuchihara, K., Iguchi, M., Huang, J., Voelker, D. R., & Toga, H. (2010). Altered lung surfactant system in a rab38-deficient rat model of Hermansky-Pudlak syndrome. *American Journal of Physiology-Lung Cellular and Molecular Physiology*, *298*(2). https://doi.org/10.1152/ajplung.00242.2009

3. Fuji, R. N., Flagella, M., Baca, M., S. Baptista, M. A., Brodbeck, J., Chan, B. K., Fiske, B. K., Honigberg, L., Jubb, A. M., Katavolos, P., Lee, D. W., Lewin-Koh, S.-C., Lin, T., Liu, X., Liu, S., Lyssikatos, J. P., O'Mahony, J., Reichelt, M., Roose-Girma, M., Sheng, Z., Sherer, T., Smith, A., Solon, M., Sweeney, Z. K., Tarrant, J., Urkowitz, A., Warming, S., Yaylaoglu, M., Shuo, Z., Zhu, H., Estrada, A. A., Watts, R. J. (2015). Effect of selective LRRK2 kinase inhibition on nonhuman primate lung. *Science Translational Medicine*, *7*(273). https://doi.org/10.1126/scitranslmed.aaa3634

4. Ahmadi Rastegar, D., & Dzamko, N. (2020). Leucine rich repeat kinase 2 and innate immunity. *Frontiers in Neuroscience*, *14*. https://doi.org/10.3389/fnins.2020.00193

5. Eguchi, T., Kuwahara, T., Sakurai, M., Komori, T., Fujimoto, T., Ito, G., Yoshimura, S. I., Harada, A., Fukuda, M., Koike, M., & Iwatsubo, T. (2018). LRRK2 and its substrate Rab GTPases are sequentially targeted onto stressed lysosomes and maintain their homeostasis. *Proceedings of the National Academy of Sciences of the United States of America*, *115*(39), E9115–E9124. https://doi.org/10.1073/pnas.1812196115

6. Prosnitz, A., Gruen, J. R., & Bhandari, V. (2013). The genetics of disorders affecting the premature newborn. *Emery and Rimoin's Principles and Practice of Medical Genetics*, 1–22. https://doi.org/10.1016/b978-0-12-383834-6.00171-3

7. Kuss, M., Adamopoulou, E., & Kahle, P. J. (2014). Interferon-γ induces leucine-rich repeat kinase LRRK2 via extracellular signal-regulated kinase ERK5 in macrophages. *Journal of Neurochemistry*, *129*(6), 980–987. https://doi.org/10.1111/jnc.12668

8. Kalogeropulou, A. F., Freemantle, J. B., Lis, P., Vides, E. G., Polinski, N. K., & Alessi, D. R. (2020). Endogenous Rab29 does not impact basal or stimulated LRRK2 pathway activity. *The Biochemical journal*, *477*(22), 4397–4423. https://doi.org/10.1042/BCJ20200458

9. Wu, C., Xue, Y., Wang, P., Lin, L., Liu, Q., Li, N., Xu, J., & Cao, X. (2014). IFN-γ primes macrophage activation by increasing phosphatase and tensin homolog via downregulation of mir-3473b. *The Journal of Immunology*, *193*(6), 3036–3044. https://doi.org/10.4049/jimmunol.1302379

10. Wang, F., Zhang, S., Jeon, R., Vuckovic, I., Jiang, X., Lerman, A., Folmes, C. D., Dzeja, P. D., & Herrmann, J. (2018). Interferon gamma induces reversible metabolic reprogramming of M1 macrophages to sustain cell viability and pro-inflammatory activity. *EBioMedicine*, *30*, 303–316. https://doi.org/10.1016/j.ebiom.2018.02.009

11. Gessani, S., & Belardelli, F. (1998). IFN-γ expression in macrophages and its possible biological significance. *Cytokine & Growth Factor Reviews*, *9*(2), 117–123. https://doi.org/10.1016/s1359-6101(98)00007-0

12. Lee, H., Flynn, R., Sharma, I., Haberman, E., Carling, P. J., Nicholls, F. J., Stegmann, M., Vowles, J., Haenseler, W., Wade-Martins, R., James, W. S., & Cowley, S. A. (2020). LRRK2 Is Recruited to Phagosomes and Co-recruits RAB8 and RAB10 in Human Pluripotent Stem Cell-Derived Macrophages. *Stem cell reports*, *14*(5), 940–955. https://doi.org/10.1016/j.stemcr.2020.04.001

13. Bowman, S. L., Bi‐Karchin, J., Le, L., & Marks, M. S. (2019). The road to lysosome‐related organelles: Insights from hermansky‐pudlak syndrome and other rare diseases. *Traffic*, *20*(6), 404–435. https://doi.org/10.1111/tra.12646

14. Kook, S., Wang, P., Meng, S., Jetter, C. S., Sucre, J. M. S., Benjamin, J. T., Gokey, J. J., Hanby, H. A., Jaume, A., Goetzl, L., Marks, M. S., & Guttentag, S. H. (2021). AP-3-dependent targeting of flippase ATP8A1 to lamellar bodies suppresses activation of YAP in alveolar epithelial type 2 cells. *Proceedings of the National Academy of Sciences of the United States of America*, *118*(20), e2025208118. https://doi.org/10.1073/pnas.2025208118